Chapter 13
Irradiation Creep and Growth

Creep is the time-dependent deformation of a metal under constant load and at high temperature ($T/T_m > 0.3$). The metal responds by elongating with a strain defined either as the nominal strain, e, calculated from the original length of the sample:

$$e = \int_{l_0}^{l} \frac{dl}{l_0} = \frac{l - l_0}{l_0}, \tag{13.1}$$

or as the true strain, ε, determined from the instantaneous length of the sample:

$$\varepsilon = \int_{l_0}^{l} \frac{dl}{l} = \ln \frac{l}{l_0} = \ln(1 + e). \tag{13.2}$$

The nominal or engineering strain is related to the nominal or engineering stress corresponding to the initial cross section of the sample, while the true strain is related to the true stress corresponding to the instantaneous cross section. The components of strain are elastic, anelastic, and plastic. Elastic strain is instantaneous, time-independent, and reversible upon release of the stress. Anelastic strain is also reversible but depends on strain rate. Plastic strain is time-dependent and irreversible and is characterized by a volume conservative change in shape or distortion of the sample. Creep refers to the time-dependent component of plastic strain.

In general, creep is a temperature-dependent process, requiring the thermal formation of vacancies and the motion of vacancies by volume or grain boundary diffusion, or the climb of dislocations over obstacles and glide along slip planes. The probability of vacancy formation and of vacancy or dislocation motion is proportional to $\exp(-Q/kT)$, where Q is the activation energy for the rate-limiting process. Increased temperature provides the thermal energy required to overcome

G.S. Was, *Fundamentals of Radiation Materials Science*,
DOI 10.1007/978-1-4939-3438-6_13

obstacles and barriers to dislocation motion. Creep is also dependent on the stress, and the nature of the stress dependence provides information about the mechanism by which it occurs. Due to the production of excess defects, irradiation can accelerate creep. Irradiation creep is not strongly dependent on temperature, primarily because the formation of vacancies and self-interstitials is provided by energetic atomic displacement rather than by thermal processes. Creep is most important in reactor applications in regions of intermediate temperature, high neutron/ion flux, and low stress. However, before we attempt to understand the role of irradiation in creep, we will review the main thermal creep mechanisms, as they will constitute the foundation for understanding irradiation creep.

13.1 Thermal Creep

In most alloys, thermal creep proceeds through a sequence of stages as shown in Fig. 13.1. In stage I, the metal undergoes strain hardening leading to a decrease in strain rate with time. At long times, necking occurs due to localized deformation resulting in an increase in the strain rate, stage III. Between these two stages is stage II, during which the creep rate is either constant or a minimum. In this region, strain hardening is balanced by recovery so that the creep rate is relatively constant. Creep in this regime is designated as steady-state or secondary creep. This is also the region of most technological importance and in which the majority of service life is spent. The variables describing plastic deformation are the shear stress, σ_s, temperature T, strain rate $\dot{\varepsilon}$, and strain ε, or time, t. The key-independent variables governing creep in metals in practical applications are temperature and stress, and the deformation mechanisms can be characterized according to these variables. As discussed in Chap. 12, Sect. 12.3, the Ashby-type deformation mechanism map can be used to describe the various deformation processes as a function of normalized stress and homologous temperature. In that chapter, we focused on the regions

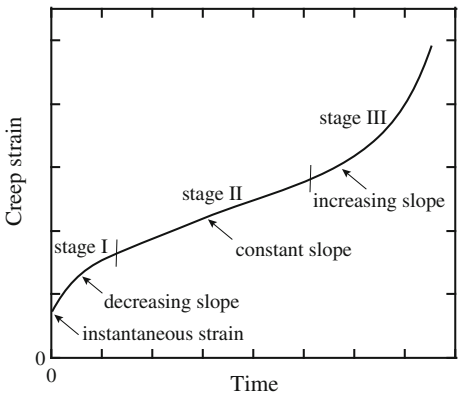

Fig. 13.1 Creep curve of a metal exhibiting the classical three stages of creep

described by plastic collapse and dislocation glide. Here, we will focus on the regions that exhibit rate-dependent plasticity, or creep.

Figure 13.2 shows a deformation mechanism map of pure nickel, for which we can develop the equations for the strain rate. The strain rate in the region of dislocation glide is given by the Orowan equation, which is a relationship between the strain rate and dislocation velocity and is determined as follows. When an edge dislocation moves completely across a slip plane, the upper half of the crystal is sheared relative to the lower half by an amount equal to one Burgers vector, b (Figs. 13.3(a)–(b)). If the dislocation moves only part way across the crystal, or a distance Δx, then the top surface is translated by an amount $b\Delta x/x$ relative to the bottom surface (Fig. 13.3(c)). So the displacement of the top half of the crystal relative to the bottom half is in relation to the fraction of the length the crystal has slipped. If the area of the slip plane is A, then $b\Delta A/A$ is the equivalent expression. The shear strain, $\varepsilon_{s,}$ is the displacement divided by the height, z, of the crystal and is given by:

$$\varepsilon_s = \frac{b\Delta A}{A}\frac{1}{z}. \tag{13.3}$$

The term zA is the volume of the crystal, V. For n dislocations of length, l, moving an average distance, $\overline{\Delta x}$, on the slip plane, the area swept out by the dislocation, ΔA, can be written as $nl\overline{\Delta x}$ giving:

$$\varepsilon_s = \frac{nbl\overline{\Delta x}}{V}. \tag{13.4}$$

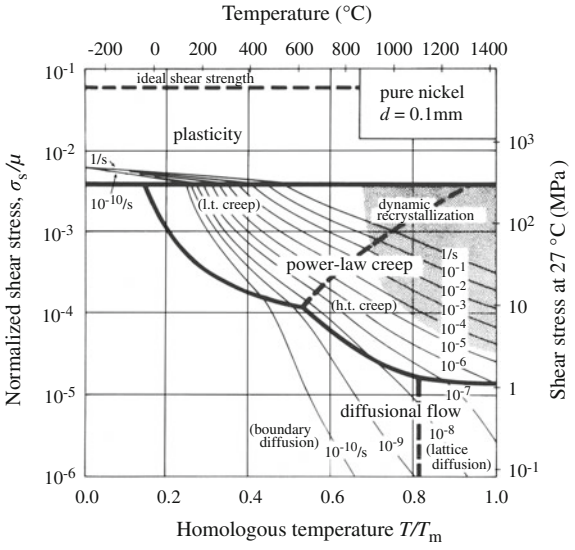

Fig. 13.2 Deformation mechanism map for pure nickel in which the strain rates and deformation mechanisms are given as a function of the normalized shear stress and the homologous temperature (after [1])

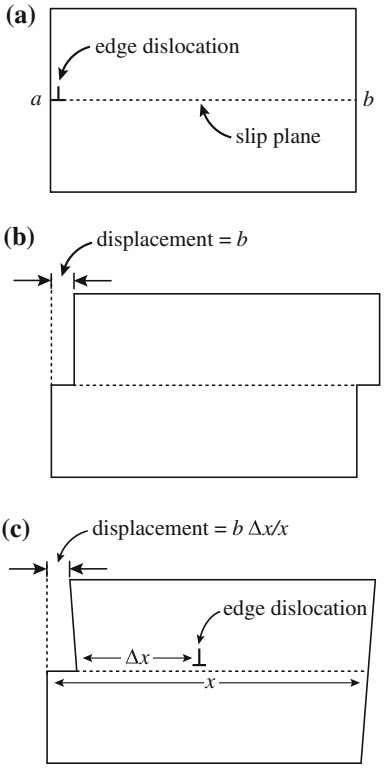

Fig. 13.3 Displacement of halves of a crystal due to passage of a dislocation along its slip plane

The term nl/V is the mobile dislocation density, ρ_m, and if the dislocations move over the distance in a time interval Δt, Eq. (13.4) can be written as a strain rate:

$$\dot{\varepsilon}_s = \rho_m b v_d, \tag{13.5}$$

where v_d is the average dislocation velocity. Equation (13.5) can be expressed in terms of the tensile strain rate, $\dot{\varepsilon}$, as

$$\dot{\varepsilon} = 1/2\rho_m b v_d, \tag{13.6}$$

where 1/2 is an approximate Schmid orientation factor.

At steady state, ρ_m is a function of stress and temperature only. As given in Eq. (7.32b), the shear stress $\sigma_s = \mu b/R$, where μ is the shear modulus and R is half the distance to the next dislocation. Since R is proportional to $\rho^{-1/2}$, then Eq. (7.32b) becomes:

$$\rho_m = \alpha\left(\frac{\sigma_s}{\mu b}\right)^2, \tag{13.7}$$

where α is a constant of order unity. The form of Eq. (13.7) depends on the process limiting plasticity at low temperature, discrete obstacles, lattice resistance, or phonon/electron drag [1].

High-temperature plasticity is described by the following:

$$\dot{\varepsilon} = c\left(\frac{\sigma_s}{\mu}\right)^n, \tag{13.8}$$

where n varies between 3 and 10 and is termed power law creep. Power law creep can occur by glide, climb-enabled glide, or Harper–Dorn creep, each process characterized by a different dependence on the stress. At very high stresses (above $10^{-3}\mu$), the strain rate is higher than predicted by power law creep and this regime is termed power law breakdown where the creep rate is given in the following form:

$$\dot{\varepsilon} = B\exp(A\sigma_s)\exp\left(\frac{-Q}{kT}\right), \tag{13.9}$$

where the activation energy, Q, often exceeds the values for self-diffusion.

At high temperatures and low stress (lower right portion of the map in Fig. 13.2), diffusional flow can drive creep. For creep controlled by lattice diffusion, the creep rate is described by:

$$\dot{\varepsilon} = \frac{A\sigma_s\Omega D_{vol}}{kTd^2}, \tag{13.10}$$

where D_{vol} is the volume diffusion coefficient and d is the grain size. When grain boundary diffusion dominates, then the creep rate varies as d^{-3}:

$$\dot{\varepsilon} = \frac{A\pi\delta_{gb}\sigma_s\Omega D_{gb}}{kTd^3}, \tag{13.11}$$

where D_{gb} is the grain boundary diffusivity and δ_{gb} is the effective thickness of the grain boundary. Equations (13.10) and (13.11) can be combined into a single equation describing creep as:

$$\dot{\varepsilon} = \frac{A\sigma_s\Omega D_{eff}}{kTd^2}, \tag{13.12}$$

where the effective diffusion coefficient, $D_{eff,}$ is given by:

$$D_{eff} = D_{vol}\left[1 + \frac{\pi\delta_{gb}}{d}\frac{D_{gb}}{D_{vol}}\right]. \tag{13.13}$$

A more complete discussion of diffusional creep will be given in Sect. 13.1.2. We will focus first on dislocation creep as this is the mechanism of primary relevance to irradiation creep.

13.1.1 Dislocation Creep

Climb and Glide

In the climb and glide model, creep is controlled by the time required for a dislocation and blocked by an obstacle, such as a void or loop, to climb to a slip plane that does not intersect the obstacle so it is free to glide. The obstacle blocking the slip of a dislocation on its glide plane causes additional dislocations generated by a nearby source to pile up behind it, as shown in Fig. 13.4. The stress fields of the dislocations overlap and create an increasing stress on the dislocation at the head of the pileup. For a solid with a mobile dislocation density, ρ_m, each dislocation, driven by a stress σ, travels a mean distance, l, by glide, resulting in a strain:

$$\varepsilon = \rho_m b l. \tag{13.14}$$

The strain rate is as follows:

$$\dot{\varepsilon} = b\frac{d}{dt}(\rho_m l) = b\rho_m \frac{dl}{dt} + bl\frac{d\rho_m}{dt}, \tag{13.15}$$

where $\bar{\upsilon} = \frac{dl}{dt}$ is the mean glide velocity, and $\frac{d\rho_m}{dt}$ is the generation rate of dislocations. We will assume that $\rho_m \bar{\upsilon} \gg l\frac{d\rho_m}{dt}$, so that creep is controlled by dislocation velocity and not dislocation generation and then the creep rate is the same as that given in Eq. (13.5), $\dot{\varepsilon} = \rho_m b \bar{\upsilon}$. However, if the moving dislocation encounters obstacles along its path, which it must overcome, then the velocity must account for the time that the dislocation is held up by the obstacle and not just its motion on the glide plane. The effective velocity can be written as:

$$\bar{\upsilon} = \frac{l}{t} = \frac{l}{t_c + t_g}, \tag{13.16}$$

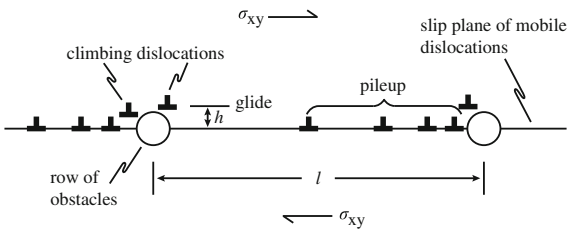

Fig. 13.4 Schematic showing the pileup of dislocations behind an obstacle on the glide plane of the dislocations

where t_g is the time spent in glide, t_c is the time spent pinned at the obstacle, and l is the distance between obstacles. As will be discussed in the next section, the dislocation overcomes the obstacle by climbing to a slip plane that bypasses the obstacle. The time required for climb is much greater than that for glide, so that Eq. (13.16) reduces to:

$$\bar{v} \approx \frac{l}{t_c}. \tag{13.17}$$

For an obstacle of height h, the time that the dislocation spends climbing to a slip plane that bypasses the obstacle can be written as:

$$t_c = \frac{h}{v_c}, \tag{13.18}$$

where v_c is the climb velocity. Substituting Eqs. (13.17) and (13.18) into Eq. (13.5) gives:

$$\dot{\varepsilon} = \rho_m b l \frac{v_c}{h}. \tag{13.19}$$

Equation (13.19) shows that determination of the creep rate amounts to determining the obstacle height and the climb velocity of the dislocation. The obstacle height is determined in the next section.

Obstacle Height

Obstacles to dislocations are often other dislocations. Equation (7.50) described the force on a moving edge dislocation due to a stationary edge dislocation. That force has two components, one in the x-direction (along the glide plane) and one in the y-direction (perpendicular to the glide plane). From Eq. (7.50), those forces are as follows:

$$F_x = \frac{\mu b^2}{2\pi(1-\nu)r}(\cos\theta\cos 2\theta) \tag{13.20a}$$

$$F_y = -\frac{\mu b^2}{2\pi(1-\nu)r}\sin\theta(2+\cos 2\theta), \tag{13.20b}$$

where we have dropped the individual designations on the Burgers vectors. Substituting for r using $y = r\cos\theta$ gives:

$$F_x = \frac{G}{y}\sin\theta\cos\theta\cos 2\theta = \frac{G}{y}g_x(\theta) \tag{13.21a}$$

$$F_y = -\frac{G}{y}\sin^2\theta(2+\cos 2\theta) = -\frac{G}{y}g_y(\theta). \tag{13.21b}$$

where $G = \dfrac{\mu b^2}{2\pi(1-\nu)}$ and $g_{x,y}(\theta)$ are functions of θ in Eqs. (13.21a) and (13.21b). The force on the moving dislocation due to the applied shear stress is $F = \sigma_{xy} b$ This force is balanced by that due to the repulsion from the stationary dislocation, Eq. (13.21a) giving:

$$\sigma_{xy} b = F_x = \frac{G}{y} g_x(\theta). \tag{13.22}$$

The blocked dislocation is also subjected to a climb force provided by Fy in Eq. (13.21b). Under this force, the dislocation will climb in a direction perpendicular to its slip plane until it reaches the point where the glide plane no longer intersects the obstacle. During its climb, the angle between the two dislocations increases starting from a value near $\theta = 0$. Referring back to the variation in force between the two dislocations as a function of angle and separation distance, r, shown in Fig. 7.32, we replot the angular dependence of the forces in Fig. 13.5 over the range $0 \le \theta \le \pi$ for a separation given by y, where the angular dependence is given by $g_{x,y}(\theta)$ in Eqs. (13.21a) and (13.21b) and $y = r\sin\theta$. Note that the restraining force between the two dislocations increases with θ initially. Once the angle reaches $\pi/8$, the restraining force is at a maximum. If the force due to the applied stress has remained in balance with the restraining force, then for values of θ above $\pi/8$, the applied stress will exceed the restraining force and the dislocation will be free to move beyond the obstacle. Setting $g_x(\theta)$ to its maximum value in Eq. (13.22) and designating the value of y at this point as the height of the obstacle, h, that must be overcome for the dislocation to be able to continue to glide yield an expression for h:

$$\begin{aligned} h = y &= \frac{G}{4\sigma_{xy} b} \\ &= \frac{\mu b}{8\pi(1-\nu)\sigma_{xy}} \sim \frac{\mu b}{16\sigma_{xy}} \quad \text{for} \quad \nu \sim 1/3. \end{aligned} \tag{13.23}$$

When there are n dislocations in a pileup against the obstacle, the stress in Eq. (13.23) is multiplied by n.

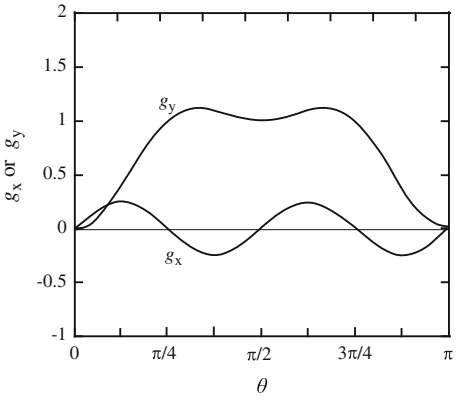

Fig. 13.5 Plot of the angular components, $g_x(\theta)$ and $g_y(\theta)$, of the force on an edge dislocation due to a stationary edge dislocation where y is the vertical separation distance between the two

Climb Velocity

An edge dislocation of Burgers vector, b, subjected to a normal stress, σ, perpendicular to the extra plane of atoms climbs in the direction normal to the slip plane. Climb occurs by absorption or emission of vacancies at the dislocation core. We will assume that this process occurs along the entire length of the dislocation line. When the solid is under an applied stress, σ (tensile is positive), the vacancy concentration in equilibrium with the dislocation is given by:

$$C(R) = C_{\mathrm{v}}^{0} \exp\left(\frac{\sigma\Omega}{kT}\right), \tag{13.24}$$

where Ω is the atomic volume and C_{v}^{0} is the equilibrium vacancy concentration in the solid, a distance R away, where R is the distance between dislocations in the solid and is given by $R = 1/\sqrt{\pi\rho_{\mathrm{d}}}$, where ρ_{d} is the dislocation density such that $\pi R^2\rho_{\mathrm{d}} = 1$ (area per dislocation × dislocations per unity area = 1). The distance R also defines the *unit cell* that reproduces, on average, the collection of ρ_{d} dislocations in the solid.

Driven by the difference in vacancy concentration between the dislocation core and the radius of the cylinder of the unit cell, defined by R, the vacancy flux to the dislocation is as follows:

$$J = 2\pi r D_{\mathrm{v}} \frac{\mathrm{d}C_{\mathrm{v}}}{\mathrm{d}r}, \tag{13.25}$$

where C_{v} is the vacancy concentration in the region $r_{\mathrm{c}} < r < R$, (r_{c} is the dislocation core radius), and is described by the diffusion equation in cylindrical coordinates:

$$\frac{1}{r}\frac{\mathrm{d}}{\mathrm{d}r}\left(r\frac{\mathrm{d}C_{\mathrm{v}}}{\mathrm{d}r}\right) = 0, \tag{13.26}$$

with boundary conditions:

$$\begin{aligned} C_{\mathrm{v}}(R) &= C_{\mathrm{v}}^{0} \exp\left(\frac{\sigma\Omega}{kT}\right) \\ C_{\mathrm{v}}(r_{\mathrm{c}}) &= C_{\mathrm{v}}^{0}. \end{aligned} \tag{13.27}$$

The solution to Eq. (13.26) subject to boundary conditions in Eq. (13.27) is as follows:

$$C_{\mathrm{v}} = C_{\mathrm{v}}^{0} - C_{\mathrm{v}}^{0}\left[1 - \exp\left(\frac{\sigma\Omega}{kT}\right)\right]\frac{\ln R/r}{\ln R/r_{c}}. \tag{13.28}$$

For $\frac{\sigma\Omega}{kT}$ small, we can approximate the exponent by $e^x \sim x + 1$, and Eq. (13.28) becomes:

$$C_v = C_v^0\left(1 + \frac{\sigma\Omega}{kT}\right)\frac{\ln R/r}{\ln R/r_c}. \tag{13.29}$$

Evaluating the gradient of the concentration profile at $r = r_c$ gives:

$$\frac{dC_v}{dr} = C_v^0\frac{\sigma\Omega}{kT}\frac{1}{\ln R/r_c}\frac{1}{r_c}, \tag{13.30}$$

and the flux, as in Eq. (13.25), becomes:

$$J_v = \frac{2\pi D_v C_v^0 \sigma\Omega}{kT\ln R/r_c}. \tag{13.31}$$

The flow of vacancies to the dislocation per unit length is $J\Omega$, or Jb^3, where $\Omega \sim b^3$. The sheet of atoms has a thickness of b so dividing by b gives the flow of volume per unit length per unit thickness, or the flow per unit distance perpendicular to the glide plane, which is just the climb velocity:

$$\begin{aligned} v_c &= \frac{2\pi D_v C_v^0 \sigma\Omega b^2}{kT\ln R/r_c} \\ &= \frac{2\pi D_{vol}\sigma b^2}{kT\ln R/r_c}, \end{aligned} \tag{13.32}$$

for $D_v C_v^0\Omega = D_{vol}$.

We now have all the elements required to derive the creep rate due to dislocation climb and glide over obstacles. Recall that the creep rate is given by Eq. (13.19) as $\dot{\varepsilon} = \rho_m bl\frac{v_c}{h}$. For the case where the dislocations are being created by Frank–Read sources, the creep rate can be expressed as the product of the Frank–Read source density, ρ_{FR}, the area swept out by the source times the Burgers vector, Ab, and the inverse of the waiting time, v_c/h or:

$$\dot{\varepsilon} = \rho_{FR}Ab\frac{v_c}{h}. \tag{13.33}$$

Substituting in for h from Eq. (13.23) and v_c from Eq. (13.32) gives:

$$\dot{\varepsilon} = \frac{16\pi^2\rho_{FR}Ab^3 D_{vol}\sigma(1-\nu)n\sigma_{xy}}{\mu bkT\ln R/r_c}. \tag{13.34}$$

The number of dislocations, n, in a pileup is given by [2]:

$$n = \frac{\pi(1-\nu)l\sigma_{xy}}{\mu b}, \tag{13.35}$$

where l is the length of the pileup, and the stress $\sigma = n\sigma_{xy}$ [2]. Substituting into Eq. (13.34) gives:

$$\dot{\varepsilon} = \frac{16\pi^2\rho_{\mathrm{FR}}AD_{\mathrm{vol}}(1-\nu)^3 l^2\sigma_{xy}^4}{\mu^3 kT\ln R/r_{\mathrm{c}}}. \tag{13.36}$$

Weertman [3, 4] suggests that the quantity $\rho_{\mathrm{FR}}Al^2$ is proportional to σ_{xy}^{-1}, yielding:

$$\dot{\varepsilon} = \frac{\mathrm{C}\pi^2 D_{\mathrm{vol}}(1-\nu)^3\sigma_{xy}^3}{\mu^3 kT\ln R/r_{\mathrm{c}}}, \tag{13.37}$$

where C is a constant. According to Eq. (13.37), the creep rate due to climb and glide is proportional to the self-diffusion coefficient and the stress to the power 3.

Climb and Annihilation

Climbing dislocations can also encounter other dislocations of opposite sign, creating an attractive force between them that drives the climb and results in mutual annihilation of the dislocations [5]. Figure 13.6 shows dislocation loops spaced apart from each other and on different slip planes. Dislocations of opposite sign will experience an attractive force that will cause them to climb toward each other and to annihilate. This is an important mechanism in that it provides a means for limiting the dislocation density in the solid. The creep rate is determined using the same

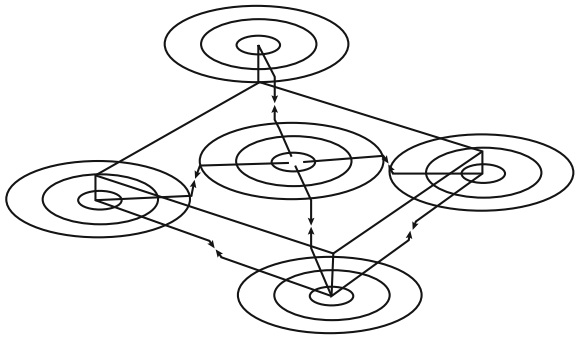

Fig. 13.6 Dislocations climbing toward each other to mutual annihilation

equation as for climb over obstacles and is caused by glide of dislocations, and piled up behind the lead dislocation, once annihilation has occurred (Fig. 13.7). That is,

$$\dot{\varepsilon} = \rho_{\mathrm{FR}} Ab \frac{\upsilon_{\mathrm{c}}}{h} = \frac{\rho_{\mathrm{FR}} Ab}{t_{\mathrm{c}}}, \tag{13.38}$$

where t_{c} is the waiting time defined by υ_{c}/h. The climb velocity is the same as determined in Eq. (13.32), but the height is now the distance between two dislocations that are climbing toward each other. Referring back to the climb force caused by a normal stress, Eq. (13.22) showed that:

$$\sigma = \frac{F_y}{b} \cong -\frac{G}{by}. \tag{13.39}$$

The rate of approach of the two dislocations of opposite sign is 2 υ_c, and combining Eq. (13.32) for υ_c and Eq. (13.39) for σ gives

$$\mathrm{d}y/\mathrm{d}t = 2\upsilon_c = -2\left(\frac{2\pi b D_{\mathrm{vol}} G}{kT \ln R/r_{\mathrm{c}} y}\right), \tag{13.40}$$

and integrating Eq. (13.40) between the limits $y = h$ at $t = 0$ and $y = 0$ at $t = t_{\mathrm{c}}$ gives:

$$t_{\mathrm{c}} = \frac{kT \ln R/r_{\mathrm{c}} h^2}{8\pi b D_{\mathrm{vol}} G}. \tag{13.41}$$

For n dislocations produced by each Frank–Read source, the waiting time per dislocation is t_{c}/n, where n is approximated by l/h [3]. Substituting Eq. (13.41) into Eq. (13.38) gives:

$$\dot{\varepsilon} = \frac{\rho_{\mathrm{FR}} Ab^2 8\pi l D_{\mathrm{vol}} G}{kT \ln R/r_{\mathrm{c}} h^3}. \tag{13.42}$$

In Eq. (13.42), A is the area swept out by the dislocation and can be approximated by πl^2, where the distance l between sources on a slip plane is given as $(h\,\rho_{\mathrm{FR}})^{-1/2}$,

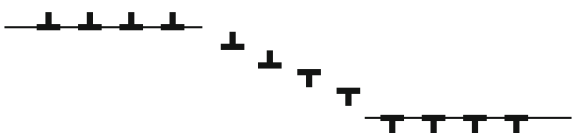

Fig. 13.7 Arrangement of a network of Frank–Read sources that produce dislocations that climb to annihilation (after [5])

where ρ_{FR} is the source density and h is the separation between sources normal to their slip planes. Substituting the expressions for A and l in Eq. (13.42) gives:

$$\dot{\varepsilon} = \frac{8\pi^2 b^2 D_{vol} G}{kT\rho_{FR}^{0.5} \ln R/r_c h^{4.5}}. \tag{13.43}$$

Substituting for h Eq. (13.23), and G (line below Eq. (13.21b)) gives:

$$\dot{\varepsilon} = \frac{C\pi^{5.5}(1-\nu)^{3.5} D_{vol} \sigma_{xy}^{4.5}}{kT\rho_{FR}^{0.5} b^{0.5} \mu^{3.5} \ln R/r_c}, \tag{13.44}$$

where C is a constant that contains the numerical terms. Note that the stress is raised to the power 4.5 rather than 3.0 in the climb to glide mode. In both climb models, the creep rate is proportional to D_{vol} or $\exp(-E_{vol}/kT)$.

13.1.2 Diffusional Creep

In the high-temperature low-stress regime of the deformation mechanism map, if we ignore the role of dislocations, then atom diffusion by way of vacancies controls creep. Consider the case of an idealized, cuboidal grain of edge length d on which a stress is applied as shown in Fig. 13.8(a). The faces will act as the sources and sinks for vacancies. Under the applied stress, vacancies will follow the paths described by the dashed lines and atoms will move in the opposite direction (solid lines). Note

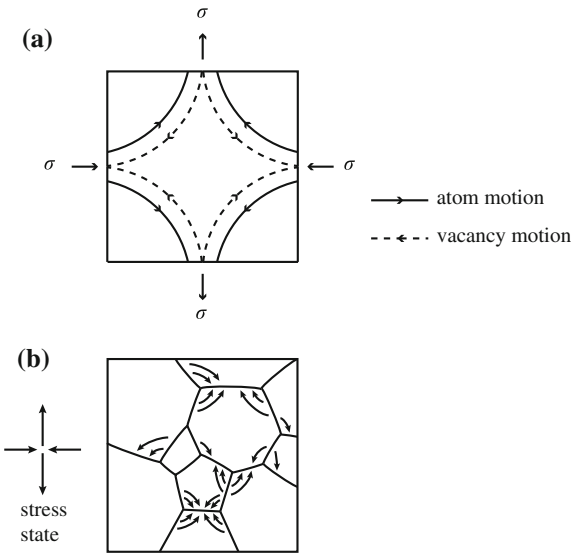

Fig. 13.8 Idealization (**a**) of a more realistic picture of vacancy and atom flow between grain faces (**b**) aligned with tensile or compressive directions of the applied stresses

that the vacancy flow is from the faces acted on by the tensile stress to those acted on by the compressive stress. The atom flow is in the opposite direction, from the faces acted on by a compressive stress to those acted on by a tensile stress. A more realistic picture of the process is shown in Fig. 13.8(b). The creation of a vacancy on the face acted on by a compressive stress, σ, due to thermal activation requires that the free energy of vacancy creation be increased by, $\sigma\Omega$, the work expended on transferring a volume Ω. A vacancy created on the face acted on by the tensile stress, σ, means that the free energy will be lowered by the same amount, $\sigma\Omega$. Therefore, at equilibrium, the vacancy concentration at the respective faces is as follows:

$$\begin{aligned} C_{\mathrm{v}}^{\mathrm{t}} &= C_{\mathrm{v}}^{0} \exp\left(\frac{\sigma\Omega}{kT}\right) \\ C_{\mathrm{v}}^{\mathrm{c}} &= C_{\mathrm{v}}^{0} \exp\left(\frac{-\sigma\Omega}{kT}\right), \end{aligned} \tag{13.45}$$

where σ is the magnitude of the stress, and the superscripts t and c refer to tensile and compressive, respectively. The vacancy flow rate, A across the area d^2 acted on by the stress is as follows:

$$A = J_{\mathrm{v}} d^2. \tag{13.46}$$

The magnitude of the vacancy flux, J_{v}, is given by Fick's law:

$$\begin{aligned} J_{\mathrm{v}} &= D_{\mathrm{v}} \frac{\mathrm{d}C}{\mathrm{d}x} \\ &\approx \kappa D_{\mathrm{v}} \frac{C_{\mathrm{v}}^{\mathrm{t}} - C_{\mathrm{v}}^{\mathrm{c}}}{d}, \end{aligned} \tag{13.47}$$

where D_{v} is the vacancy diffusion coefficient, and κ is a coefficient of proportionality between the mean vacancy diffusion path and the cube edge d. Substituting Eqs. (13.45) and (13.47) into Eq. (13.46) gives:

$$A = D_{\mathrm{v}} C_{\mathrm{v}}^{0} \kappa d \left[\exp\left(\frac{\sigma\Omega}{kT}\right) - \exp\left(\frac{-\sigma\Omega}{kT}\right)\right]. \tag{13.48}$$

Recognizing that $D_{\mathrm{vol}} = D_{\mathrm{v}} C_{\mathrm{v}}^{0} \Omega$ and that the difference in exponentials can be written using the hyperbolic sine function, Eq. (13.48) becomes:

$$A = \frac{2\kappa d D_{\mathrm{vol}}}{\Omega} \sinh(\sigma\Omega/kT). \tag{13.49}$$

The strain is just the atom volume, Ω, transferred to the compressive faces per unit area (d^2) divided by the dimension, d:

$$\varepsilon = \frac{\Omega}{d^2}\frac{1}{d}. \tag{13.50}$$

Since the flow rate of vacancies to the boundary is A, then the strain rate becomes:

$$\dot{\varepsilon} = A\frac{\Omega}{d^3} = \frac{2\kappa D_{\text{vol}}}{d^2}\sinh(\sigma\Omega/kT), \tag{13.51}$$

and for $\sigma\Omega/kT$ small (~ 1), the sinh term can be approximated by its argument, yielding:

$$\dot{\varepsilon} = B_{\text{vol}}\frac{D_{\text{vol}}\sigma\Omega}{d^2kT}, \tag{13.52}$$

where B_{vol} is the constant 2κ. Note that the creep rate is controlled by stress to the power $n = 1$ and is inversely proportional to the square of the grain diameter. The temperature dependence is governed by the volume diffusion coefficient D_{vol} exp ($-E_{\text{vol}}/kT$) and is identical to that due to dislocation creep described in the last section. Extension of this mechanism to polycrystals [6] results in the exact same expression. Diffusional creep due to volume or lattice diffusion of atoms by way of vacancies is termed Nabarro–Herring (N–H) creep after the individuals who first derived the creep expression [7, 8].

At temperatures below the range where Nabarro–Herring creep occurs, grain boundary diffusion dominates mass transport. Coble [9] first derived an expression for grain boundary-dominated diffusion assuming spherical grains, yielding the following expression:

$$\dot{\varepsilon} = B_{\text{gb}}\frac{D_{\text{gb}}\delta_{\text{gb}}\sigma\Omega}{\pi d^3kT}. \tag{13.53}$$

In this expression, D_{gb} is the grain boundary diffusion coefficient, δ_{gb} is the grain boundary width, and the constant $B_{\text{gb}} \sim 148$ [6]. Note that while the stress dependence is the same as for N–H creep, the grain size dependence is d^{-3} rather than d^{-2}. Due to the nature of grain boundary diffusion versus volume diffusion, Coble creep will dominate at lower temperatures and N–H creep will dominate at higher temperatures, and both will contribute in the intermediate temperature range. The diffusional creep rate can therefore be described by a common equation:

$$\dot{\varepsilon} = B\frac{\sigma\Omega}{d^2kT}D_{\text{eff}}, \tag{13.54}$$

and as was shown earlier, D_{eff} is the effective diffusion coefficient given by:

$$D_{\text{eff}} = D_{\text{vol}}\left(1 + \frac{\pi}{d}\frac{D_{\text{gb}}\delta_{\text{gb}}}{D_{\text{vol}}}\right), \tag{13.55}$$

and the constant $B = 14$ [6]. It follows then that grain boundary diffusion will contribute to the creep rate at larger values of $D_{\text{gb}}/D_{\text{vol}}$ and for smaller grain sizes d.

13.2 Irradiation Creep

Irradiation significantly increases the creep rate over that due to thermal creep or induces creep in temperature regimes where thermal creep is negligible. Both stainless steels and zirconium alloys exhibit irradiation creep rates that are significantly larger than thermal creep rates at the same temperature. In fact, at light water reactor core temperatures, thermal creep is negligible, but the irradiation creep rate can exceed $10^{-6}\ \text{s}^{-1}$. Irradiation increases the numbers of interstitials and vacancies in the solid, but the effect of this increase is not merely to accelerate thermal creep. In fact, as will be shown, irradiation does not accelerate diffusional creep rates. Rather, irradiation creep needs to be understood in the context of enhanced defect production, the application of a stress, and the developing irradiation microstructure. The formation and growth of loops and voids play important roles in the creep process. As will be shown, the stress-induced nucleation of dislocation loops and the bowing of dislocation lines by stress-assisted preferential absorption of interstitials can account for the transient portion of the creep behavior, but climb and glide are required to explain steady-state creep. The following sections present the mechanisms responsible for creep in metals under irradiation and their dependencies on the independent variables of dose rate, temperature, and stress as well as the developing microstructure.

13.2.1 Stress-Induced Preferential Nucleation of Loops (SIPN)

The application of an external stress can enhance the probability of interstitial loops nucleating on planes with a preferred orientation. Interstitial loops will be more likely to nucleate on planes perpendicular to an applied tensile stress than parallel to the stress. Vacancy loops will be less likely to nucleate on planes perpendicular (non-aligned) to the tensile stress and more likely to nucleate on planes parallel (aligned) to the stress. In either case, such preferential loop nucleation will cause the solid to increase in length in the direction of the applied tensile stress (Fig. 13.9). This process is termed the *stress-induced preferential nucleation*, SIPN mechanism

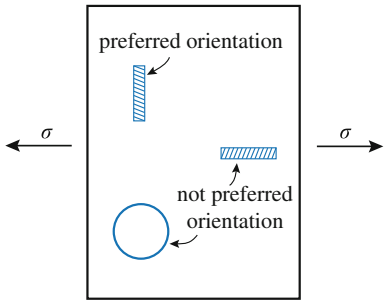

Fig. 13.9 Schematic of the influence of stress on the nucleation of dislocation loops

of irradiation creep [10]. If f is the excess fraction of aligned interstitial loops, then the concentration of aligned loops, N_{AL}, [11] is as follows:

$$N_{\mathrm{AL}} = 1/3(1-f)N_{\mathrm{L}} + fN_{\mathrm{L}}, \tag{13.56}$$

and the concentration of non-aligned loops, N_{NL}, is as follows:

$$N_{\mathrm{NL}} = 2/3(1-f)N_{\mathrm{L}}, \tag{13.57}$$

where N_{L} is the total loop concentration. The excess fraction of aligned interstitial loops is determined as follows.

If n interstitials are required before the interstitial aggregate is able to form an interstitial loop, then the probability that such an aggregate will form, p, in response to a normal stress is as follows:

$$p_i = \exp\frac{\sigma_i n\Omega}{kT} \Bigg/ \sum_{j=1}^{n_0} \exp\frac{\sigma_j n\Omega}{kT}, \tag{13.58}$$

where the subscript i refers to the ith orientation of n_0 possible loop orientations, and the number of loops in the ith orientation is as follows:

$$N_{\mathrm{L}}^{i} = p_i N_{\mathrm{L}}. \tag{13.59}$$

Defining f_i as the excess fraction of interstitial loops in the ith orientation, then:

$$p_i N_{\mathrm{L}} = \frac{1}{n_0}\left(1 - \sum_{j=1}^{n_0} f_j\right) N_{\mathrm{L}} + f_i N_{\mathrm{L}}, \quad i = 1\ldots n_0, \tag{13.60}$$

giving:

$$f_i = \left(\exp\frac{\sigma_i n\Omega}{kT} - 1\right) \Bigg/ \sum_{j=1}^{n_0} \exp\frac{\sigma_j n\Omega}{kT}. \tag{13.61}$$

We can simplify the description by reducing the n_0 possible orientations to the three orthogonal directions. Then, for a uniaxial tensile stress orthogonal to the $i = 1$ orientation, the other two orthogonal orientations ($i = 2, 3$) will have $p_2 = p_3 = 0$, and:

$$f_1 = \left(\exp\frac{\sigma_1 n\Omega}{kT} - 1\right) \Big/ \left(\exp\frac{\sigma_1 n\Omega}{kT} + 2\right), \tag{13.62}$$

and $f_2 = f_3 = 0$.

Using the result from Eq. (13.62), the creep strain due to the asymmetry in the loop population is as follows:

$$\varepsilon = 2/3\left[\pi r_L^2 b N_{AL} - 1/2\pi r_L^2 b N_{NL}\right]. \tag{13.63}$$

Substituting for N_{AL} and N_{NL} from Eqs. (13.56) and (13.57) gives:

$$\varepsilon = 2/3 f \pi r_L^2 b N_L, \tag{13.64}$$

where b is the Burgers vector, and r_L is the average loop radius. The creep rate is obtained by taking the time derivative of the creep strain given in Eq. (13.64), yielding:

$$\dot{\varepsilon} = 4/3 f b \pi r_L N_L \dot{r}_L, \tag{13.65}$$

and defining $\rho_L = 2\pi r_L N_L$ as the loop line length per unit volume gives:

$$\dot{\varepsilon} = 2/3 f b \rho_L \dot{r}_L. \tag{13.66}$$

If the argument of the exponential term in the expression for f in Eq. (13.62) is small compared to 1, then the exponent can be replaced by $\exp(x) \sim x + 1$, yielding:

$$f = \frac{\sigma n\Omega}{3kT}, \tag{13.67}$$

where the subscript on the stress is dropped, and Eq. (13.66) becomes:

$$\dot{\varepsilon} = \frac{2}{9}\frac{\sigma n b\Omega}{kT}\rho_L \dot{r}_L. \tag{13.68}$$

Note that the creep rate is proportional to stress and the loop growth rate, $\dot{r}_L$. Brailsford and Bullough [10] have shown that the creep rate can be related to swelling if the irradiated microstructure consists of only loops and voids as sinks and the absorption rate of vacancies by voids equals the absorption rate of interstitials by loops. In Eq. (13.65), the product of $2\pi r_L b$ (edge area of loop of thickness b) and $\dot{r}_L$ is the interstitial volume added to the loop. Multiplying by N_L loop/unit

volume gives the volume fraction increase of the loop due to the net absorption of interstitials. If this is balanced by a corresponding and equal net absorption of vacancies to voids to produce a fractional swelling rate, $\dot{S}$, then Eq. (13.65) becomes:

$$\dot{\varepsilon} = 2/3 f \dot{S}. \tag{13.69}$$

Substituting for f using Eq. (13.67) for the case where n is small yields:

$$\dot{\varepsilon} = \frac{2}{9}\frac{\sigma n b \Omega}{kT}\dot{S}, \tag{13.70}$$

and generalizing for the case where the total dislocation density is $\rho = \rho_L + \rho_N$ gives:

$$\dot{\varepsilon} = \frac{2}{9}\frac{\sigma n \Omega}{kT}\frac{\rho_L}{\rho}\dot{S}. \tag{13.71}$$

A more general treatment [12] of strain due to an anisotropic distribution of loops describes the strain in a volume due to a continuous distribution of dislocation loops [13] using the strain tensor:

$$\varepsilon_{ij} = \sum_{k=1}^{M} \frac{\rho^k A^k n_i^k b_j^k}{\Delta V}, \tag{13.72}$$

The equation describes the strain ε caused by M groups of loops in a volume ΔV, where the k^{th} group of loops all have the same Burgers vector b, area A, normal vector n, and number density ρ. The subscript i denotes x-, y-, z-directions of the loop normal vector, and subscript j denotes the contribution of loop Burgers vectors to the x-, y-, z-directions. M represents individual grains within a polycrystal. For a single grain:

$$\varepsilon_{ij}^k = \frac{N^k \pi \left(\frac{d}{2}\right)^2 n_i^k b_j^k}{\Delta V}, \tag{13.73}$$

where N^k is the total number of the k^{th} loop in the volume ΔV, and d is the measured loop diameter. Solution of Eq. (13.73) requires an expression for N^k. Taking as an example, irradiation of T91 at 500 °C to 1 dpa during application of a tensile stress of 180 MPa, the $a\langle 100\rangle$ loop distribution is shown in Fig. 13.10(a) and plotted in Fig. 13.10(b). Note that loops form preferentially with their normal in the direction of the tensile stress according to the following equation:

$$N^k/N = \alpha - \beta\theta^k, \tag{13.74}$$

where the constants α and β are fitting constants, and θ is defined as the angle between the loop normal and the tensile axis as shown in Fig. 13.11. Substituting

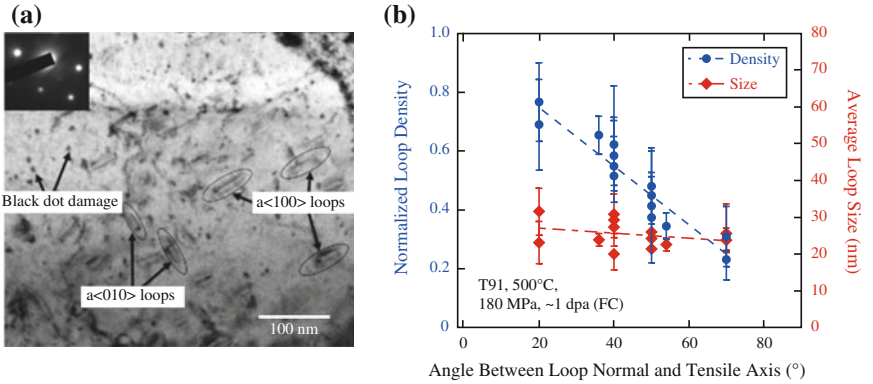

Fig. 13.10 (**a**) TEM image of $a\langle 100\rangle$ edge-on loops with $g = \langle 110\rangle$ on the $\langle 100\rangle$ zone axis and (**b**) loop anisotropy plot of the loop density and size following irradiation at 500 °C with a tensile stress of 180 MPa (after [12])

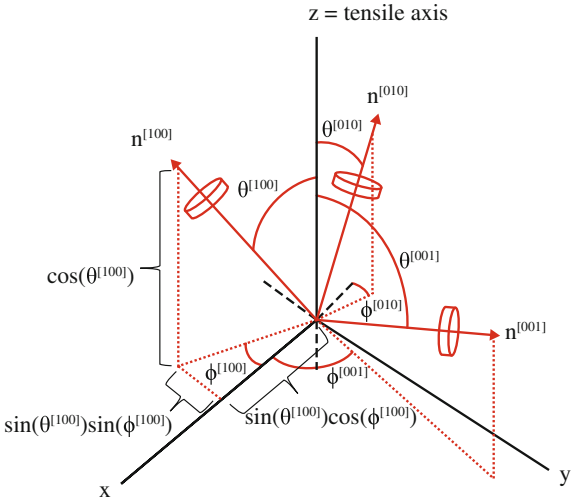

Fig. 13.11 Schematic of the normal vectors n^k of three sets of dislocation loops, where k = [100], [010], and [001]. The components of the $n^{[100]}$ are defined in the Cartesian coordinate system where the z-axis is the tensile axis (after [12])

the expression for N^k in Eq. (13.74) into Eq. (13.73) and simplifying [12] yields the strain in direction i:

$$\varepsilon_i = b\rho\pi\left(\frac{d}{2}\right)^2 \frac{\int_{\phi=0}^{\pi/2}\int_{\theta=0}^{\pi/2} n_i(\alpha-\beta\theta)\mathrm{d}\phi\mathrm{d}\theta}{\int_{\phi=0}^{\pi/2}\int_{\theta=0}^{\pi/2}(\alpha-\beta\theta)\mathrm{d}\phi\mathrm{d}\theta} - \frac{1}{3}\varepsilon_{\mathrm{vol}}. \tag{13.75}$$

The last term in Eq. (13.75) ensures volume conservation of creep by subtracting one-third of the volumetric expansion caused by dislocation loops from the strain of the three primary directions.

In the example provided, the creep strain due to anisotropy of the dislocation loops observed in the samples was found to account for only about 4.4 % of the total strain measured in the sample. This observation was consistent with previous works that claimed that strain due to anisotropy in the dislocation loops was much lower than the total measured strain [14], suggesting that another deformation mechanism must be driving the irradiation creep behavior.

Whether SIPN can accurately account for the observed creep strains is a matter of considerable debate. Matthews and Finnis [14] reviewed the arguments for and against SIPN and noted that while observations have supported an increase in preferred loop orientation with tensile stress, the magnitude of the measured creep strain is higher than can be accounted for by preferred orientation by a factor of 2–4, even if n is assumed to be large (10–30). The greatest limitation of the model is that once a loop is nucleated, the strain rate is determined by the irradiation dose, but is independent of stress. Thus, creep should continue if the stress is removed once nucleation has been completed. Also, if nucleation occurs before the stress is applied, then creep should not occur. Clearly, SIPN cannot account for all of the observed creep, but it may be a viable mechanism for a portion of the observed creep strain rate. A compliment to loop nucleation is preferential absorption of defects by loops caused by the applied stress, discussed in the next section.

13.2.2 Stress-Induced Preferential Absorption (SIPA)

At steady state, there are several distinct processes that may result in creep of a solid under irradiation and stress. They are (1) the transfer of atoms from planes parallel to the applied stress to those perpendicular to the applied stress, (2) the glide of dislocations on planes inclined to the stress direction, and (3) the climb and glide of dislocations due to the interstitial bias of the dislocation. The first is termed *stress-induced preferential absorption* (SIPA), and the second process is termed *preferred absorption glide* (PAG) [15]. PAG results from preferred absorption (SIPA) but is an additional component to the creep strain since it describes the glide contribution to the creep strain, whereas SIPA describes only the climb contribution to creep strain. The third mechanism is creep strain from the climb and glide process due to the net absorption of interstitials on dislocations of all orientations (i.e., unassisted by stress) and is essentially the same process as the climb and glide model described in Sect. 13.1 but for the case where the defect source is the excess interstitials. Note that this process is tied to swelling as the corresponding net excess of vacancies accumulates at cavities causing swelling.

The origin of the preferred absorption is the interaction between the dislocation and defects. In conventional SIPA, the origin is the elastic interaction between the

long-range stress field of the dislocation and that of the defect. Other origins for SIPA are anisotropic diffusion and elastodiffusion. While differing in the details of the origin of the interaction, all of these mechanisms result in a preferred absorption of interstitials by dislocations.

The flux of excess interstitials absorbed by dislocations with orientation described by j and density ρ_{j} is as follows:

$$J_j = \rho_j \Omega \left(z_{\mathrm{i}}^{\mathrm{d}j} D_{\mathrm{i}} C_{\mathrm{i}} - z_{\mathrm{v}}^{\mathrm{d}j} D_{\mathrm{v}} C_{\mathrm{v}} + z_{\mathrm{v}}^{\mathrm{d}j} D_{\mathrm{v}} C_{\mathrm{v}}^{\mathrm{d}j} \right), \tag{13.76}$$

where $z_{\mathrm{i,v}}^{\mathrm{d}j}$ are the capture efficiencies of dislocations of orientation, j, D_{iv} are the diffusion coefficients, and C_{iv} are the bulk concentrations of interstitials and vacancies. The variable, $C_{\mathrm{v}}^{\mathrm{d}j}$, is the vacancy concentration in equilibrium with a dislocation of orientation j. For a uniaxial tensile stress where $j = 1$:

$$C_{\mathrm{v}}^{\mathrm{d}1} = C_{\mathrm{v}}^{0} \exp\left(\frac{\sigma \Omega}{kT} \right) \tag{13.77}$$

$$C_{\mathrm{v}}^{\mathrm{d}2} = C_{\mathrm{v}}^{\mathrm{d}3} = C_{\mathrm{v}}^{0}. \tag{13.78}$$

The interstitial flux, J_j, can also be related to the climb velocity as follows:

$$J_j = b \rho_j \upsilon_j, \tag{13.79}$$

where ρ_j is the density of dislocations with their planes perpendicular to j. Substituting for J_j from Eq. (13.79) into Eq. (13.76) and solving for υ_{j} gives:

$$\upsilon_j = \frac{\Omega}{b} \left(z_{\mathrm{i}}^{\mathrm{d}j} D_{\mathrm{i}} C_{\mathrm{i}} - z_{\mathrm{v}}^{\mathrm{d}j} D_{\mathrm{v}} C_{\mathrm{v}} + z_{\mathrm{v}}^{\mathrm{d}j} D_{\mathrm{v}} C_{\mathrm{v}}^{\mathrm{d}j} \right). \tag{13.80}$$

Substituting Eq. (13.80) into Eq. (13.5) gives the total creep rate as:

$$\dot{\varepsilon}_{\mathrm{j}} = \Omega \left(z_{\mathrm{i}}^{\mathrm{d}j} D_{\mathrm{i}} C_{\mathrm{i}} - z_{\mathrm{v}}^{\mathrm{d}j} D_{\mathrm{v}} C_{\mathrm{v}} + z_{\mathrm{v}}^{\mathrm{d}j} D_{\mathrm{v}} C_{\mathrm{v}}^{\mathrm{d}j} \right) \rho_j. \tag{13.81}$$

But Eq. (13.81) also includes contributions due to void swelling. That component of the strain is just one-third of the volumetric swelling, or $\varepsilon = 1/3(\varepsilon_1 + \varepsilon_2 + \varepsilon_3)$, and the swelling strain rate, $\dot{\varepsilon}_{\mathrm{S}}$, is as follows:

$$\dot{\varepsilon}_{\mathrm{S}} = \frac{\Omega}{3} \sum_{n=1}^{3} \left(z_{\mathrm{i}}^{\mathrm{d}n} D_{\mathrm{i}} C_{\mathrm{i}} - z_{\mathrm{v}}^{\mathrm{d}n} D_{\mathrm{v}} C_{\mathrm{v}} + z_{\mathrm{v}}^{\mathrm{d}n} D_{\mathrm{v}} C_{\mathrm{v}}^{\mathrm{d}n} \right) \rho_n. \tag{13.82}$$

The creep by climb due to preferential absorption of interstitials at dislocations is then:

$$\begin{aligned}\dot{\varepsilon}_j = {} & \Omega(z_{\mathrm{i}}^{\mathrm{d}j} D_{\mathrm{i}} C_{\mathrm{i}} - z_{\mathrm{v}}^{\mathrm{d}j} D_{\mathrm{v}} C_{\mathrm{v}} + z_{\mathrm{v}}^{\mathrm{d}j} D_{\mathrm{v}} C_{\mathrm{v}}^{\mathrm{d}j})\rho_j \\ & - \frac{\Omega}{3} \sum_{n=1}^{3} \left(z_{\mathrm{i}}^{\mathrm{d}n} D_{\mathrm{i}} C_{\mathrm{i}} - z_{\mathrm{v}}^{\mathrm{d}n} D_{\mathrm{v}} C_{\mathrm{v}} + z_{\mathrm{v}}^{\mathrm{d}n} D_{\mathrm{v}} C_{\mathrm{v}}^{\mathrm{d}n} \right) \rho_n .\end{aligned} \tag{13.83}$$

For dislocations distributed isotropically among the three orthogonal directions:

$$\rho_1 = \rho_2 = \rho_3 = \rho/3. \tag{13.84}$$

Substituting Eqs. (13.77) and (13.78) for the equilibrium vacancy concentration and Eq. (13.84) for the dislocation density into Eq. (13.83) for the stress direction $j = 1 = A$ (aligned dislocations) gives:

$$\dot{\varepsilon}_{\mathrm{climb}} = \frac{2}{9} \Omega \rho \left\{ \underbrace{\left[\Delta z_{\mathrm{i}}^{\mathrm{d}} D_{\mathrm{i}} C_{\mathrm{i}} - \Delta z_{\mathrm{v}}^{\mathrm{d}} D_{\mathrm{v}} C_{\mathrm{v}} \right]}_{\mathrm{SIPA}} + \underbrace{D_{\mathrm{v}} C_{\mathrm{v}}^{0} \left[z_{\mathrm{v}}^{\mathrm{dA}} \exp\left(\frac{\sigma \Omega}{kT} \right) - z_{\mathrm{v}}^{\mathrm{dN}} \right]}_{\mathrm{PE}} \right\}, \tag{13.85}$$

where $\Delta z_{\mathrm{i,v}}^{\mathrm{d}} = z_{\mathrm{i,v}}^{\mathrm{dA}} - z_{\mathrm{i,v}}^{\mathrm{dN}}$, and $z_{\mathrm{i,v}}^{\mathrm{dA}}$ denotes the capture efficiency of aligned dislocations, and $z_{\mathrm{i,v}}^{\mathrm{dN}}$ denotes the capture efficiency of non-aligned dislocations ($j = 2$). The first term in square brackets is the dislocation climb creep rate due to preferential absorption of interstitials, or SIPA:

$$\dot{\varepsilon}_{\mathrm{SIPA}} = \frac{2}{9} \Omega \rho \left[\Delta z_{\mathrm{i}}^{\mathrm{d}} D_{\mathrm{i}} C_{\mathrm{i}} - \Delta z_{\mathrm{v}}^{\mathrm{d}} D_{\mathrm{v}} C_{\mathrm{v}} \right]. \tag{13.86}$$

The second term in square brackets is the dislocation climb creep rate due to preferred emission, PE [15], of vacancies:

$$\dot{\varepsilon}_{\mathrm{PE}} = \frac{2}{9} \Omega \rho D_{\mathrm{v}} C_{\mathrm{v}}^{0} \left[z_{\mathrm{v}}^{\mathrm{dA}} \exp\left(\frac{\sigma \Omega}{kT} \right) - z_{\mathrm{v}}^{\mathrm{dN}} \right]. \tag{13.87}$$

If the differences in capture efficiencies (preference) of the dislocations in different orientations were removed, i.e., $\Delta z_{\mathrm{i}}^{\mathrm{d}} = \Delta z_{\mathrm{v}}^{\mathrm{d}} = 0$, then the first term disappears and the creep rate is then due solely to thermal processes.

13.2.3 Climb and Glide Due to Preferential Absorption Glide (PAG)

While SIPA provides a mechanism for creep by dislocation climb, dislocations can also contribute to creep by glide if they are able to overcome obstacles in their slip plane by the climb process [15]. Under an applied stress, pinned dislocations will glide until they reach a configuration where the restoring force due to line tension is balanced by the applied stress. Since dislocations are pinned, creep is limited to the elastic stress given by $\varepsilon = \sigma/E$. Climb enables the dislocation to overcome the initial pinning points. The released segments bow out between new pinning points until, again, the line tension balances the applied stress. Figure 13.12 shows the process by which dislocation segments bow out between pinning points, are released from the pinning points, and are then pinned again. Each cycle of climb and glide to pinning results in an elastic deflection in addition to the strain due to climb, which together, account for the total creep strain in the solid, all the while, the dislocation network maintains its configuration. This mechanism has also been referred to as "transient creep" because of its occurrence at low dose. However, since the dislocation lines can continue to bow out after climbing over pinning points, it can also account for steady-state creep.

Similar to Eq. (13.19), the creep rate due to climb and glide can be written as:

$$\dot{\varepsilon}_{\mathrm{CG}} = \varepsilon \frac{\upsilon_{\mathrm{c}}}{l}, \tag{13.88}$$

where ε is the strain due to elastic deflection, υ_{c} is the climb velocity, and l is the distance between pinning points. When pinning is caused by the network dislocation density, l is given by $l = 1/\sqrt{\pi\rho_{\mathrm{d}}}$, and ρ_{d} is the dislocation density. Equation (13.88) then becomes:

$$\dot{\varepsilon}_{\mathrm{CG}} = \varepsilon(\pi\rho_{\mathrm{d}})^{1/2}\upsilon_{\mathrm{c}}. \tag{13.89}$$

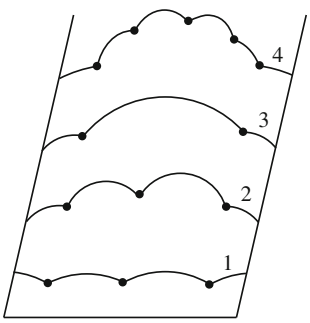

Fig. 13.12 Schematic of glide by dislocation bowing and the pinning and unpinning of dislocation segments

The climb velocity can be determined from Eq. (13.80) by adding and subtracting the velocity component due to volumetric swelling:

$$\begin{aligned} v_j = \frac{\Omega}{b}\Bigg[&\left(z_{\mathrm{i}}^{\mathrm{d}j} D_{\mathrm{i}} C_{\mathrm{i}} - z_{\mathrm{v}}^{\mathrm{d}j} D_{\mathrm{v}} C_{\mathrm{v}} + z_{\mathrm{v}}^{\mathrm{d}j} D_{\mathrm{v}} C_{\mathrm{v}}^{\mathrm{d}j}\right) \\ &- \frac{1}{3\rho_j} \sum_{n=1}^{3} \left(z_{\mathrm{i}}^{\mathrm{d}n} D_{\mathrm{i}} C_{\mathrm{i}} - z_{\mathrm{v}}^{\mathrm{d}n} D_{\mathrm{v}} C_{\mathrm{v}} + z_{\mathrm{v}}^{\mathrm{d}n} D_{\mathrm{v}} C_{\mathrm{v}}^{\mathrm{d}n}\right) \rho_n \Bigg] \\ &+ \frac{\Omega}{3b\rho_j} \sum_{n=1}^{3} \left(z_{\mathrm{i}}^{\mathrm{d}n} D_{\mathrm{i}} C_{\mathrm{i}} - z_{\mathrm{v}}^{\mathrm{d}n} D_{\mathrm{v}} C_{\mathrm{v}} + z_{\mathrm{v}}^{\mathrm{d}n} D_{\mathrm{v}} C_{\mathrm{v}}^{\mathrm{d}n}\right) \rho_n . \end{aligned} \tag{13.90}$$

The physical meanings of the terms in Eq. (13.90) are as follows. The first term in square brackets is the climb velocity due to all processes contributing to vacancy and interstitial absorption and vacancy emission. The second term in the square brackets is the climb due to net point defect absorption and emission at dislocations attributable only to swelling. Subtracting this term from the first term yields the net result, enclosed in square brackets, being the climb velocity due only to the volume-conserving processes of stress-induced preferential absorption and to preferred vacancy emission. The last term in Eq. (13.90) is the dislocation climb velocity due to isotropic swelling. It is the terms in square brackets that are responsible for the climb and glide process in the absence of swelling. Using Eq. (13.84) and the average velocity of the dislocations given by:

$$v = \frac{|v_1| + |v_2| + |v_3|}{3}, \tag{13.91}$$

equation (13.90) becomes:

$$v = \frac{\Omega}{3b}\left\{\left|z_{\mathrm{i}}^{\mathrm{d}1} D_{\mathrm{i}} C_{\mathrm{i}} - z_{\mathrm{v}}^{\mathrm{d}1} D_{\mathrm{v}} C_{\mathrm{v}} + z_{\mathrm{v}}^{\mathrm{d}1} D_{\mathrm{v}} C_{\mathrm{v}}^{\mathrm{d}1}\right| + 2\left|z_{\mathrm{i}}^{\mathrm{d}2} D_{\mathrm{i}} C_{\mathrm{i}} - z_{\mathrm{v}}^{\mathrm{d}2} D_{\mathrm{v}} C_{\mathrm{v}} + z_{\mathrm{v}}^{\mathrm{d}2} D_{\mathrm{v}} C_{\mathrm{v}}^{\mathrm{d}2}\right|\right\}. \tag{13.92}$$

When preferential absorption and preferential emission occur without swelling, the number of interstitials absorbed must be balanced by the number of vacancies absorbed, so:

$$\left(z_{\mathrm{i}}^{\mathrm{d}1} D_{\mathrm{i}} C_{\mathrm{i}} - z_{\mathrm{v}}^{\mathrm{d}1} D_{\mathrm{v}} C_{\mathrm{v}} + z_{\mathrm{v}}^{\mathrm{d}1} D_{\mathrm{v}} C_{\mathrm{v}}^{\mathrm{d}1}\right) = 2\left(z_{\mathrm{i}}^{\mathrm{d}2} D_{\mathrm{i}} C_{\mathrm{i}} - z_{\mathrm{v}}^{\mathrm{d}2} D_{\mathrm{v}} C_{\mathrm{v}} + z_{\mathrm{v}}^{\mathrm{d}2} D_{\mathrm{v}} C_{\mathrm{v}}^{\mathrm{d}2}\right), \tag{13.93}$$

and Eq. (13.92) becomes:

$$v = \frac{2}{3}\frac{\Omega}{b}\left(z_{\mathrm{i}}^{\mathrm{d}1} D_{\mathrm{i}} C_{\mathrm{i}} - z_{\mathrm{v}}^{\mathrm{d}1} D_{\mathrm{v}} C_{\mathrm{v}} + z_{\mathrm{v}}^{\mathrm{d}1} D_{\mathrm{v}} C_{\mathrm{v}}^{\mathrm{d}1}\right). \tag{13.94}$$

Substituting the climb velocity given in Eq. (13.94) into the creep equation for climb and glide, Eq. (13.89) gives:

$$\dot{\varepsilon}_{\mathrm{CG}} = \frac{2}{3}\frac{\varepsilon}{b}\Omega(\pi\rho_{\mathrm{d}})^{1/2}\left(z_{\mathrm{i}}^{\mathrm{d1}}D_{\mathrm{i}}C_{\mathrm{i}} - z_{\mathrm{v}}^{\mathrm{d1}}D_{\mathrm{v}}C_{\mathrm{v}} + z_{\mathrm{v}}^{\mathrm{d1}}D_{\mathrm{v}}C_{\mathrm{v}}^{\mathrm{d1}}\right). \tag{13.95}$$

After some manipulation of Eq. (13.95), Mansur [15] showed that the climb and glide creep rate can be written as:

$$\dot{\varepsilon}_{\mathrm{CG}} = \frac{4}{9}\frac{\varepsilon\Omega}{b}\Omega(\pi\rho_{\mathrm{d}})^{1/2}D_{\mathrm{i}}C_{\mathrm{i}}\Delta z_{\mathrm{i}}^{\mathrm{d}}, \tag{13.96}$$

where $\Delta z_{\mathrm{i}}^{\mathrm{d}}$ is defined after Eq. (13.85). Note that in both Eqs. (13.86) and (13.96), the term $\Delta z_{\mathrm{i}}^{\mathrm{d}}$ appears, which represents the difference in capture efficiencies between aligned and non-aligned dislocations, and is therefore dependent on stress. Mansur writes $\Delta z_{\mathrm{i}}^{\mathrm{d}} = \Delta z_{\mathrm{i}}'\varepsilon$ (where $\Delta z_{\mathrm{i}}'$ is independent of stress) so that $\dot{\varepsilon}_{\mathrm{SIPA}} \propto \varepsilon$ and $\dot{\varepsilon}_{\mathrm{CG}} \propto \varepsilon^2$, and since $\varepsilon = \sigma/E$,we have $\dot{\varepsilon}_{\mathrm{SIPA}} \propto \sigma$ and $\dot{\varepsilon}_{\mathrm{CG}} \propto \sigma^2$. Also, as shown in Sect. 5.1.3, the term C_{i} is proportional to the defect production rate, K_0, for sink-dominated cases and to $K_0^{1/2}$ for recombination-dominated cases. It should also be noted that since there is no need for a net preferential absorption of interstitials at all edge dislocations, creep can proceed in the absence of swelling.

13.2.4 Climb and Glide Driven by Dislocation Bias

The preceding analysis describes creep that is driven by stress-induced preferential absorption of interstitials at dislocations. The creep rate has both climb and glide components, and the creep process is governed by dislocation segment bowing following climb to free the segment from the pinning points. Here, we consider creep that is driven by the dislocation bias rather than preferential absorption. Clearly in order for there to be a net absorption of interstitials by dislocations requires that there is an equivalent net absorption of vacancies by other sinks in the solid. These sinks are assumed to be voids. Creep due to the excess absorption of interstitials at dislocations is equivalent to the thermal creep climb and glide mechanisms discussed in Sect. 13.2, but with interstitial absorption replacing vacancy absorption. For this case, we return to Eq. (13.19), which expresses the creep rate in terms of the climb velocity, υ_{c}, and the obstacle height, h. Equation (13.79) gives the climb velocity in terms of the absorption flux of interstitials at dislocations. For climb due solely to dislocation bias, Eq. (13.76) for the interstitial flux becomes:

$$J = \rho_{\mathrm{m}}\Omega\left[z_{\mathrm{i}}^{\mathrm{d}}D_{\mathrm{i}}C_{\mathrm{i}} - z_{\mathrm{v}}^{\mathrm{d}}D_{\mathrm{v}}C_{\mathrm{v}}^{\mathrm{d}}\right], \tag{13.97}$$

and substituting the expression for J in Eq. (13.97) into Eq. (13.79) and solving for υ_c gives:

$$\upsilon_c = \frac{\Omega}{b}\left[z_i^d D_i C_i - z_v^d D_v C_v^d\right]. \tag{13.98}$$

Equation (13.98) also can be obtained directly from Eq. (13.90) by neglecting thermal emission, $C_v^{dj} \sim 0$, and requiring that the zs for dislocations do not have an orientation dependence, so that $z_v^{dj} = z_v^d$ *and* $z_i^{dj} = z_i^d$. The obstacle height is given in Eq. (13.23), and in the case of a dislocation pileup against an obstacle, the stress σ_{xy} is replaced by $n\sigma_{xy}$ where n is the number of dislocations in the pileup and is given by Eq. (13.35). Substituting Eq. (13.98) for υ_c, Eq. (13.23) for h, and Eq. (13.35) for n into Eq. (13.19) gives:

$$\dot{\varepsilon} = \frac{\rho_m l^2 \Omega 8\pi^2 (1-\nu)^2 \sigma_{xy}^2}{(\mu b)^2}\left[z_i^d D_i C_i - z_v^d D_v C_v^d\right]. \tag{13.99}$$

When creep is driven by swelling, the absorption rate of interstitials at dislocations is balanced by the same absorption rate of vacancies by voids:

$$\rho_m (J_i^d - J_v^d) = A_v^V - A_i^V = \frac{1}{\Omega}\frac{\Delta \dot{V}}{V}. \tag{13.100}$$

Substituting Eq. (13.100) into Eq. (13.99) gives:

$$\dot{\varepsilon} = \frac{\rho_m}{\rho_d}\frac{8\pi^2 l^2 (1-\nu)^2 \sigma_{xy}^2}{(\mu b)^2}\frac{\Delta \dot{V}}{V}, \tag{13.101}$$

where the term ρ_m/ρ_d is the fraction of the dislocation density that is mobile and can contribute to creep. It should also be noted that irradiated metals often do not exhibit pileups at obstacles. In this case, the number of dislocations in a pileup, n, is set equal to 1 and the creep rate is proportional to the stress. Wolfer et al. [16] showed that when Frank loops are the obstacles, the creep rate is proportional to stress to the power $n = 1$.

13.2.5 Transient Creep

Creep can occur prior to the achievement of steady state by the vacancy and interstitial concentrations. Such creep is referred to as *transient creep*. Three transient creep processes are of greatest importance: *glide-induced transient absorption, start-up-induced transient absorption*, and *cascade creep*.

Glide-Induced Transient Absorption

In climb and glide creep, the climb process is the limiting step as glide occurs extremely rapidly. In fact, the glide process is so rapid that steady-state concentrations of point defects cannot be maintained at the dislocation. As a result, the dislocation absorbs both vacancies and interstitials rapidly in an effort to re-establish the steady-state point defect diffusion profiles at its new location [17]. However, vacancies and interstitials are not absorbed in equal numbers, and the imbalance in absorption rate gives rise to a form of transient creep termed glide-induced transient absorption. Figure 5.3 in Chap. 5 shows that at steady state, the bulk vacancy concentration exceeds the interstitial concentration by orders of magnitude. Consequently, the flow of vacancies to the dislocation causes an increment of positive climb, releasing the dislocation from an obstacle and producing creep by glide. Figure 13.13 shows the increment of climb caused by excess vacancy absorption prior to achievement of steady-state diffusion profiles. The initial climb shown in the positive direction is the transient vacancy climb, and the negative climb at longer times ($Dt = 10^8$ nm^2) is the bias-driven interstitial climb. If the transient positive climb is large enough to escape the barrier, the dislocation glides to the next barrier. If the transient climb is inadequate, the steady-state climb eventually reverses the dislocation motion, and escape occurs in the negative direction. Once steady state has been achieved, then climb is controlled by the small net excess of interstitials due to stress-induced preferential absorption described in the preceding section. This form of transient climb can cause high creep rates at low temperatures, where the steady-state vacancy concentration is high, as long as the temperature is not too low so that vacancy diffusion is limiting.

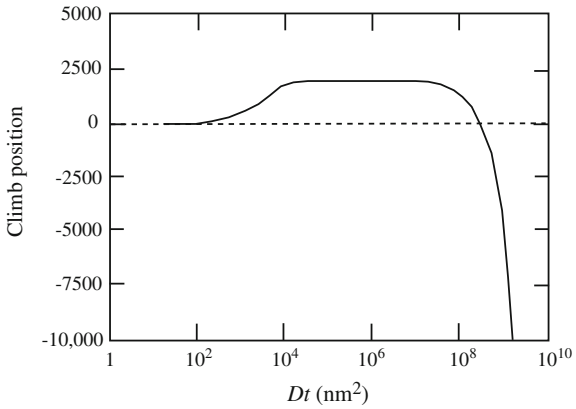

Fig. 13.13 Dislocation climb for a unit length of dislocation in units normalized to the steady-state vacancy concentration divided by 10^{18}. The diffusion coefficients are in units of nm^2/s, and a steady-state climb rate corresponding to 1 % of the total interstitial flux is assumed (after [17])

Start-Up-Induced Transient Absorption

Significant creep can also occur at low temperatures coincident with the start of the irradiation. This creep process, referred to as start-up-induced transient absorption, occurs by the absorption of interstitials prior to steady state when interstitials are mobile, but vacancy diffusion is too slow for them to interact with the dislocations [18]. Referring again to Fig. 5.3, at the start of irradiation at low temperature, the concentrations of both vacancies and interstitials increase linearly with time until interstitials begin to be absorbed at sinks. At this point in time, defined by the time constant τ_2, the interstitial concentration reaches a quasi-steady state, while the vacancy concentration continues to climb. The continued buildup of vacancies causes recombination to occur, resulting in a decrease in the interstitial concentration and a slower rate of vacancy buildup with time. With additional increase in the vacancy concentration, recombination dominates the loss process (at $t = \tau_4$) causing a steeper decline in the interstitial loss rate and a smaller rate of vacancy buildup. Eventually, steady state is reached when the vacancy concentration is high enough that vacancies interact with sinks.

The contribution of interstitials to creep during this start-up transient can be estimated by determining the number of excess interstitials, N_i, that are absorbed by the dislocations in each time interval in Fig. 5.3. For example, in the time interval τ_4–τ_2, the number of interstitials produced is K_0 (τ_4–τ_2), and the number remaining is $K_0/K_{is}C_s$, so the number absorbed by the dislocation is as follows:

$$N_i = K_0(\tau_4 - \tau_2) - K_0/K_{is}C_s. \tag{13.102}$$

Using the same analysis, estimates can be made for the number of interstitials absorbed during the time interval τ_3–τ_4, or until steady state is reached, at which point the transient ends. Interstitial absorption results in climb-enabled glide as described by Eq. (13.96), with N_i substituted for C_i. Figure 13.14 shows that the

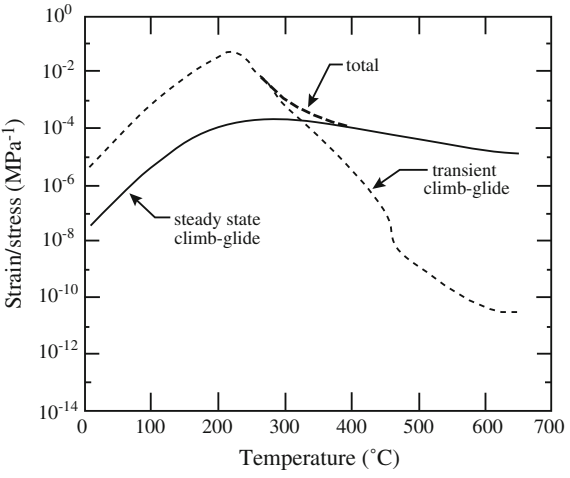

Fig. 13.14 Creep deformation per unit stress as a function of temperature for austenitic alloys using the conventional climb-enabled glide model (steady-state condition) and the start-up-induced transient absorption model (from [18])

total creep strain in austenitic stainless steels can be dominated by start-up-induced transient absorption at temperatures into the 300 °C range and near the 200 °C range for ferritic alloys. As such, it is an important mechanism of creep at low temperature and during the start-up phase of an irradiation.

Cascade Creep

One of the simplest transient creep models is based on the effect of stress on the displacement spike volume. As described by Brinkman and Wiedersich [19], if a load is applied to a solid during the occurrence of a displacement spike, then elastic strain in the spike region is relaxed locally and frozen in. The strain rate from this process is given by:

$$\dot{\varepsilon}_{\text{cas}} = \varepsilon_{\text{e}} V_{\text{cas}} \alpha N \sigma_{\text{s}} \phi, \tag{13.103}$$

where the elastic strain $\varepsilon_{\text{e}} = \sigma/E$, V_{cas} is the volume of the cascade, α is the number of spikes per neutron scattering event, N is the atom number density in the solid, σ_{s} is the neutron scattering cross section, and ϕ is the fast neutron flux. Matthews and Finnis [14] noted that this creep rate underestimates the observed irradiation creep in neutron-irradiated structural materials. However, since defect generation does not occur continuously over space and time, and not all defects escape the damage region, strain caused by cascade effects may be important to consider. A dislocation segment will make climb excursions in response to fluctuations in the local vacancy concentration caused by a nearby cascade. During an excursion, there is a probability that the segment will be unpinned. Mansur [20] accounted for cascade effects in the climb-enabled glide model by replacing υ_{c}/h in Eq. (13.19) by the release frequency of pinned dislocation segments, ω:

$$\dot{\varepsilon} = \rho b l \omega, \tag{13.104}$$

where:

$$\omega = \sum_{j-1}^{h} R_j F_j, \tag{13.105}$$

and F_j is the frequency with which a dislocation segment climbs to a height of at least h:

$$F_j = 4\pi N \sigma_{\text{s}} \phi \int_0^{\infty} \rho^2 P_j \mathrm{d}r, \tag{13.106}$$

and P_j is the probability of climb of j or greater. The term, $R_{j,}$ is the probability of finding a dislocation a distance jb from the unpinning point and is given by:

$$R_j = \rho_j/\rho. \tag{13.107}$$

The release frequencies and hence the creep rates determined using this model are comparable to those from preferred absorption-driven climb or swelling-driven climb [20].

13.2.6 Loop Unfaulting

Another possible interaction between an applied stress and interstitial loops that could produce creep strain is loop unfaulting. As discussed in Chap. 7, dislocation loops grow in size and eventually become unstable and unfault to become part of the dislocation network. This process is equivalent to the production of mobile dislocations which may then participate in the creep process by SIPA, PAG, or climb and glide driven by interstitial bias. The maximum radius to which a loop can grow, $R_{\max}$, is governed by the loop density and is given by:

$$\frac{4\pi}{3}\rho_{\mathrm{L}}R_{\max}^{3}=1. \tag{13.108}$$

When loops interact, they coalesce and contribute to the network dislocation density. Interaction between individual dislocations and loops results in loop unfaulting that also contributes to the network (see Chap. 12, Sect. 12.3). As the dislocation density increases, the rate of loop interaction with the network increases and the loop radius is limited to a value of the order of the network mesh length, $\rho_{\mathrm{N}}^{-1/2}$, where ρ_{N} is the network dislocation density. Loop unfaulting can contribute to irradiation creep strain since the presence of a stress will assist the nucleation of the unfaulting dislocations with favorable orientations resulting in an increased probability of unfaulting. The application of a shear stress in the plane of the loops will induce a greater number of loops to shear in the direction favored by the stress to produce a net shear of the crystal, which will appear as creep. If ρ is the total dislocation density and ρ_{s} is the number of dislocation loops lying on a plane for which the shear stress is a maximum, then the number of loops shearing in that direction is given by Lewthwaite [21] as follows:

$$\rho_1=\frac{\rho_{\mathrm{s}}\exp\left(\dfrac{\pi R_{\mathrm{c}}^{2}b\sigma}{kT}\right)}{\exp\left(\dfrac{\pi R_{\mathrm{c}}^{2}b\sigma}{kT}\right)+\exp\left(-\dfrac{\pi R_{\mathrm{c}}^{2}b\sigma}{kT}\right)}, \tag{13.109}$$

where R_{c} is the critical loop size for unfaulting [the maximum value is given by Eq. (13.108)], and σ is the stress. The number of loops shearing in the opposite direction is $\rho_2 = \rho_{\mathrm{s}}-\rho_1$, and the strain due to the loop unfaulting is then:

$$\varepsilon=\bar{A}b_{\mathrm{s}}(\rho_1-\rho_2), \tag{13.110}$$

where $\bar{A}$ is the average loop area, and b_s is the magnitude of the Burgers vector of the reaction producing the strain. Substituting in for ρ_1 and ρ_2 in Eq. (13.110) and averaging the strain over all possible loop orientations (which gives a factor of 1/30) yields:

$$\varepsilon = \frac{\rho \bar{A} b_s}{30}\left[\frac{\exp\left(\frac{\pi R_c^2 b\sigma}{kT}\right) - \exp\left(-\frac{\pi R_c^2 b\sigma}{kT}\right)}{\exp\left(\frac{\pi R_c^2 b\sigma}{kT}\right) + \exp\left(-\frac{\pi R_c^2 b\sigma}{kT}\right)}\right]. \tag{13.111}$$

The term in brackets can be written as the hyperbolic tangent of the argument, giving:

$$\varepsilon = \frac{\rho \bar{A} b_s}{30}\tanh\left(\pi R_c^2 b\sigma/kT\right). \tag{13.112}$$

If the argument is small compared to 1, then $\tanh x \sim x$ and Eq. (13.112) becomes:

$$\varepsilon = \frac{\rho \bar{A} b_s}{30}\pi R_c^2 b\sigma/kT. \tag{13.113}$$

If loop growth is driven by swelling, then $\rho \bar{A} b_s$ is replaced with $\Delta \dot{V}/V$, the loop volume $\pi R_c^2 b$ is equated with the volume of the defects in the loop, $n_c \Omega$, and the term $\frac{k_L^2}{k_L^2 + k_N^2}$ is added to account for the network dislocation density as well, to yield the creep rate in terms of the swelling rate:

$$\dot{\varepsilon} = \frac{\Delta \dot{V}}{V}\frac{k_L^2}{k_L^2 + k_N^2}\frac{\pi R_c^2 b\sigma/kT}{30}. \tag{13.114}$$

Matthews and Finnis [14] noted that the unfaulting radius is large in austenitic alloys and the creep rate can be significant, but because of the small critical loop size in bcc metals, the contribution will be small.

13.2.7 Recovery Creep

All of the irradiation creep mechanisms discussed thus far allow for or contribute to the growth of the dislocation density, but do not account for the removal of dislocations, as must occur during creep. Matthews and Finnis [14] expressed the rate of change in dislocation density in terms of the creep rate as follows:

$$\dot{\rho} = \frac{\dot{\varepsilon}}{bl} - 2\rho^{3/2} v_c, \tag{13.115}$$

where l is the mean dislocation glide length, and v_c is the climb velocity. The first term is the production rate of dislocations due to creep, obtained from Eq. (13.14), and the second term is the loss due to annihilation. Taking the steady-state limit of $\dot{\rho} = 0$, the steady-state creep rate is expressed in terms of the dislocation density as follows:

$$\dot{\varepsilon} = 2bl\rho^{3/2}v_c. \tag{13.116}$$

The stress dependence is determined by the dislocation density, the climb velocity, and the slip length. The dislocation density varies with stress according to Eq. (13.7) (in which the term, α, appears in the denominator inside the brackets) $\rho = \dfrac{\sigma^2}{\alpha^2\mu^2b^2}$ and contributes a σ^3 term to the creep rate given in Eq. (13.116). For stress-induced preferential absorption, we have from Eq. (13.86):

$$v_{\mathrm{SIPA}} = \frac{2}{9}\frac{\Omega}{b}\left(z_i^d D_i C_i - z_v^d D_v C_v + z_v^d D_v C_v^d\right), \tag{13.117}$$

substituting into Eq. (13.116) and equating $\Omega = b^3$ gives:

$$\dot{\varepsilon} = \frac{4}{9}\frac{\sigma^3 l}{\alpha^3\mu^3}\left(z_i^d D_i C_i - z_v^d D_v C_v + z_v^d D_v C_v^d\right). \tag{13.118}$$

If l is fixed by impenetrable obstacles and is therefore independent of stress, then the stress dependence of the creep rate is σ^3. However, if l is determined by the dislocation density, then substituting for l from Eq. (13.88) and expressing the dislocation density in terms of stress, Eq. (13.7) gives:

$$\dot{\varepsilon} = \frac{4}{9}\frac{\sigma^2 b}{\sqrt{\pi}\alpha^2\mu^2}\left(z_i^d D_i C_i - z_v^d D_v C_v + z_v^d D_v C_v^d\right), \tag{13.119}$$

where the stress dependence is σ^2, which is the same stress dependence as in preferential absorption climb and glide given by Eq. (13.99).

13.2.8 *Diffusional Creep: Why There Is No Effect of Irradiation*

All of the mechanisms of irradiation creep discussed thus far are based on the actions of dislocations. The reason is that while diffusional creep is a viable thermal creep mechanism, it is unaffected by irradiation and can be understood as follows. Consider the discussion of Nabarro–Herring creep in Sect. 13.1.2. There it was shown that creep is driven by a difference in the equilibrium vacancy concentrations at the grain boundaries oriented parallel to the tensile and compressive stress directions, Eq. (13.45). Under irradiation, Eq. (13.47) is modified to include interstitials:

$$J_v = D_v \frac{dC_v}{dx} - D_i \frac{dC_i}{dx} \approx \kappa D_v \frac{C_v^t - C_v^c}{d} - \kappa D_i \frac{C_i^t - C_i^c}{d}. \tag{13.120}$$

Substituting in for C_v^t and C_v^c from Eq. (13.45) and for C_i^t and for C_i^c using the same equations but with the signs on the arguments of the exponential terms reversed because of the opposite effect of stress on interstitials gives:

$$\begin{aligned} J_v = \kappa D_v & \frac{C_v^0 \exp\left(\frac{\sigma\Omega}{kT}\right) - C_v^0 \exp\left(-\frac{\sigma\Omega}{kT}\right)}{d} \\ - \kappa D_i & \frac{C_i^0 \exp\left(-\frac{\sigma\Omega}{kT}\right) - C_i^0 \exp\left(\frac{\sigma\Omega}{kT}\right)}{d}. \end{aligned} \tag{13.121}$$

Applying the approximation that the term $\frac{\sigma\Omega}{kT}$ is small compared to 1 yields:

$$J_v = \frac{2\kappa\sigma\Omega}{dkT}(D_v C_v^0 + D_i C_i^0) \approx \frac{2\kappa\sigma\Omega}{dkT} D_v C_v^0, \tag{13.122}$$

where the approximation is due to the fact that although D_i is greater than D_v, C_v^0 is much greater than C_i^0 The vacancy flux given in Eq. (13.122) is the same as that in Eq. (13.47), and thus, there is no effect of irradiation on Nabarro–Herring creep. The reason is that the creep rate is driven by the *difference* in the equilibrium values of defects at the grain boundaries, and these values do not depend on the concentration of vacancies or interstitials in the matrix. Irradiation simply serves to increase the flow of defects to each boundary equally without a change in the net amount. The same argument applies to Coble creep. As such, diffusional creep is unaffected by irradiation and does not contribute to irradiation creep.

13.2.9 Comparison of Theory with Creep Data

Much like thermal creep, irradiation creep is characterized by an initially high creep rate that declines with irradiation dose or fluence and transitions into steady-state or secondary creep that is generally linear with dose. The difference between irradiation creep and thermal creep is in the magnitudes. A general equation for irradiation creep is as follows:

$$\varepsilon = A\left[1 - \exp\left(-\frac{\phi t}{C}\right)\right]\sigma + B_0 \sigma^n \phi^m t, \tag{13.123}$$

where the first term is transient creep, and the second term is steady-state creep. A typical irradiation creep curve exhibiting transient and steady-state regimes

is shown in Fig. 13.15 for 20 % CW 316 stainless steel. Irradiation creep rates are much larger than those due solely to thermal processes. Of the mechanisms discussed, SIPN accounts best for the transitory nature of the primary creep regime, but cannot explain steady-state creep. In the absence of swelling, steady-state irradiation creep can be described by the second term in Eq. (13.123). Data show that the creep strain rate is proportional to neutron fluence ($m = 1$), Fig. 13.16, and also proportional to stress ($n = 1$). The creep strain is then often written as the effective strain per unit of effective stress per dpa:

$$\dot{\bar{\varepsilon}}/\bar{\sigma} = B_0, \tag{13.124}$$

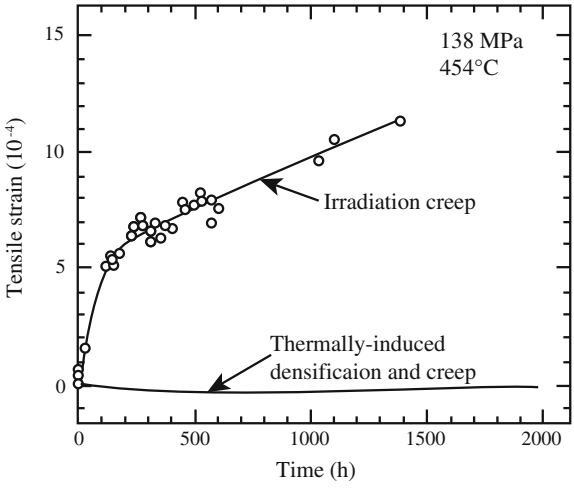

Fig. 13.15 Irradiation creep in 20 % cold-worked 316 stainless steel irradiated in EBR-II (after [22])

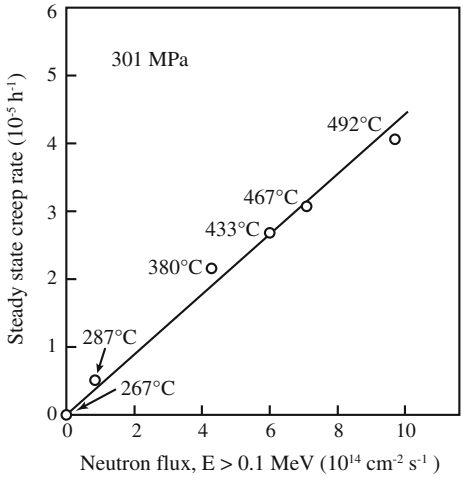

Fig. 13.16 Creep rate as a function of neutron flux in annealed 09Kh16NM3B irradiated in BR-10 (after [22])

where $\dot{\bar{\varepsilon}}$ is the effective strain rate, $\bar{\sigma}$ is the effective stress, and B_0 is the creep compliance. Note that the "rate" implied by the dot over $\bar{\varepsilon}$ is per dpa, not time. The creep compliance, B_0, is independent of composition, starting state, dpa rate, and temperature over the range of reactor relevant conditions.

There are significant data to support the irradiation creep rate behavior described by Eq. (13.124), and some of the most convincing data provided in Fig. 13.17 gives a value of B_0 of $\sim 3\times10^{-6}$ MPa^{-1} dpa^{-1}. The dependence of creep rate on stress to the power $n = 1$ provides support for the SIPA mechanism of creep. Note also that the strains appear to be independent of temperature over the range studied, supporting irradiation creep as the mechanism behind the strain rate rather than thermal creep, which has a very steep temperature dependence. The creep rate has also been observed to vary as $\phi^{1/2}$ at low temperature, yielding a B_0 dependence on flux of (dpa rate)$^{-1/2}$. In ferritic–martensitic alloy T91, the creep rate is found to follow an approximately linear stress dependence in the low-stress regime, and a transition to a strong dependence on stress ($n \sim 14$) in the high-stress regime, Fig. 13.18, indicative of a transition from irradiation-induced creep by either SIPA or PAG at low stress, to power law breakdown at high stress [23].

When void swelling occurs during creep, the steady-state creep rate is proportional to the swelling rate and the relationship is described by the following empirical equation [22]:

$$\dot{\bar{\varepsilon}}/\bar{\sigma} = B_0 + D\dot{S}, \tag{13.125}$$

where D is the creep-swelling coupling coefficient and $\dot{S}$ is the instantaneous volumetric swelling rate per dpa. While Eq. (13.125) is empirical, the relationship can also be determined from theory as well. Recall Eq. (8.122) for swelling in which

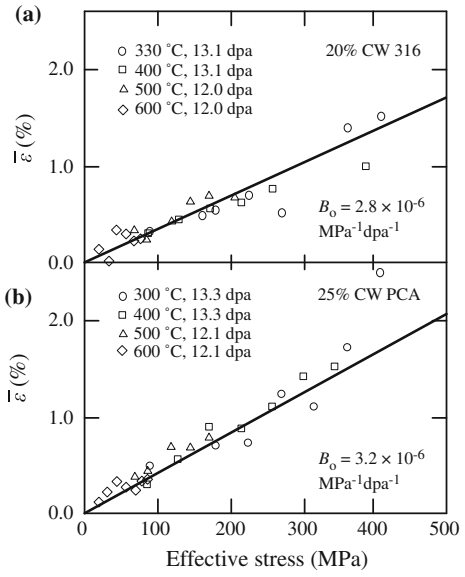

Fig. 13.17 Dependence of the normalized creep strain on effective stress in (**a**) 20 % CW and (**b**) 25 % CW PCA, over a range of temperatures and within a narrow dose range of 12.0–13 3 dpa [22]

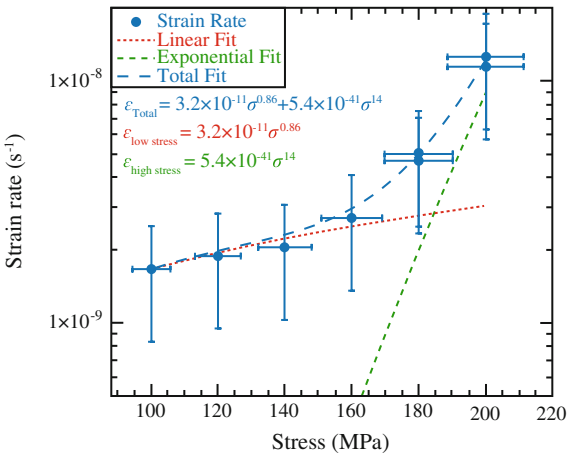

Fig. 13.18 Stress dependence of irradiation creep rate of T91 at 450 °C, 1.7×10^{-6} dpa/s and fits to the data in the low and high-stress regimes (after [23])

thermal emission of vacancies is negligible and recombination is negligible. Assuming that the only point defect sinks are voids and dislocations and that the dislocation sink strength is much greater than the void sink strength, then Eq. (8.122) becomes:

$$\dot{R} = \frac{K_0(z_i - z_v)\Omega}{Rz_i z_v \rho_d}, \tag{13.126}$$

and the void swelling rate is as follows:

$$\dot{S} = 4\pi R^2 \dot{R}\rho_v = \frac{4\pi R K_0 \rho_v \Omega\left(z_i^d - z_v^d\right)}{z_i^d z_v^d \rho_d}. \tag{13.127}$$

Substituting the expression for C_i from Eqs. (5.31) and (5.67) into Eq. (13.86) for SIPA creep, where only the first term is retained, the creep rate can be written as:

$$\dot{\varepsilon}_{SIPA} = \frac{2}{9}\frac{\Omega\rho_d \Delta z_i^d K_0}{z_i^d \rho_d}, \tag{13.128}$$

and the ratio of the creep rate to the swelling rate is as follows:

$$\frac{\dot{\varepsilon}_{SIPA}}{\dot{S}} = \frac{2}{9}\delta\frac{z_v^d \rho_d}{4\pi R_V \rho_V}, \tag{13.129}$$

where $\delta = \dfrac{\Delta z_i^d}{\left(z_i^d - z_v^d\right)}$. The linear dependence of creep rate on void swelling applies as well to climb–glide creep.

Some of the earliest and most convincing results supporting this coupling between creep and swelling are shown in Fig. 13.19 for annealed 304 SS irradiated in EBRII. The coupling was further supported by the strong correlation between creep and swelling in pressurized tube experiments in the PHENIX reactor (Fig. 13.20). Typical values for D are $\sim 10^{-2}$ MPa^{-1}. Garner [22] presents a more complete description of the dependencies of B_0 and D on the various parameters affecting creep. While the creep compliance and the coupling term are not strict constants, the relation between creep, stress, flux, and swelling is well described by

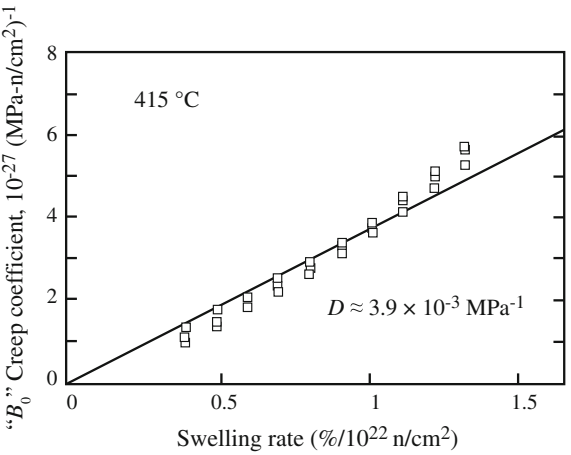

Fig. 13.19 Correlation of irradiation creep coefficients with swelling rates for annealed 304L stainless steel irradiated in EBR-II (after [22])

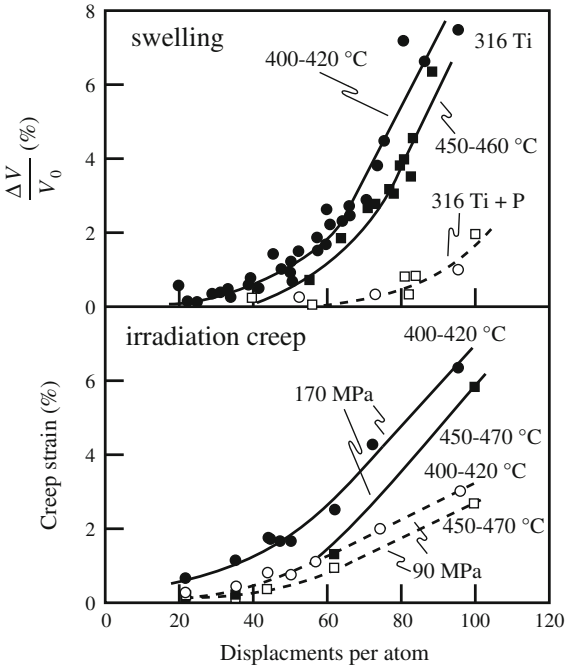

Fig. 13.20 Swelling and creep strains in two French steels irradiated as pressurized tubes in the PHENIX reactor (after [22])

Eq. (13.125).The complexity of irradiation creep and its strong dependence on the irradiated microstructure is illustrated by the observation by Garner et al. [24] that at high levels of irradiation dose, the irradiation creep rate can drop to zero. This phenomenon is illustrated in Fig. 13.21 in which instantaneous creep coefficient in a stainless steel irradiated in EBR-II at 550 °C is observed to increase to a maximum and then drop to zero at high dose. Note that deformation has not stopped, rather at the point where the creep compliance goes to zero, the deformation can be totally accounted for by the strain due to swelling, $\varepsilon_{linear} = \varepsilon_{swelling}/3$. This occurrence has its origin in the development of the dislocation network and loop microstructure. Under irradiation and an applied stress, creep is sensitive to the anisotropy of the dislocation microstructure and accounts for processes such as SIPA and PAG, in addition to SIPN. In the absence of swelling, the degree of anisotropy increases with dose. When voids begin to form, they consume vacancies and the matching interstitial flux to dislocations overwhelms that in the void-free, dislocation-dominated case, causing an increase in the creep rate that is coincident with the onset of swelling. When voids become the dominant sink, they absorb both vacancies and interstitials in large numbers. The consequence is twofold: a reduction in the creep rate caused by the small excess interstitial flux to dislocations and a saturation in swelling due to low excess vacancy absorption. The dependence of creep on composition and metallurgical condition is largely determined by the response of swelling to those factors in the regime where creep is driven by swelling.

13.2.10 Irradiation-Modified Deformation Mechanism Map

The deformation mechanism map for 316 stainless steel can be modified to account for irradiation creep. Figure 13.22 shows the deformation map for 316 SS constructed in a manner identical to that for Fig. 12.31, but at a strain rate of 10^{-10} s^{-1} [25]. At this strain rate, irradiation creep is observable in the intermediate

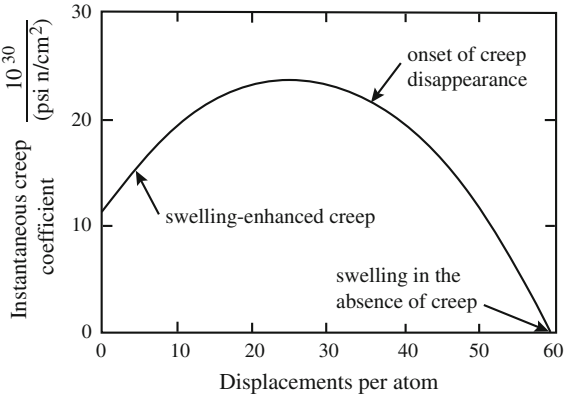

Fig. 13.21 The instantaneous creep coefficient determined from strain measurements of pressurized tubes of stainless steel, irradiated in the EBR-II reactor at 550 °C (after [22])

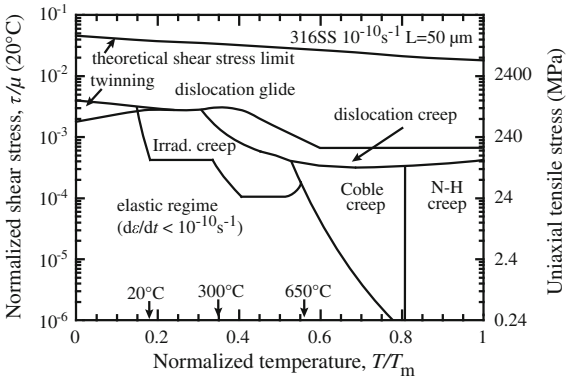

Fig. 13.22 Deformation mechanism map for 316 stainless steel irradiated to 1 dpa for a plastic strain rate of 10^{-10} s^{-1} (after [25])

temperature regime. Below 20 °C, interstitial mobility drops and so does the irradiation creep rate. Above about 600 °C, Coble creep is the dominant creep mechanism. The irradiation creep regime, therefore, lies at intermediate temperature and intermediate stresses and can be described by the constitutive equation for irradiation creep strain given by Eq. (13.125) in which the first term is due to dislocation creep (lower temperature portion of irradiation creep regime) and the second term is due to swelling-driven creep (higher temperature portion). The net effect of irradiation is to extend rate-dependent deformation to lower stresses.

13.3 Irradiation Growth and Creep in Zirconium Alloys

In addition to swelling and creep, there is another phenomenon that leads to strains in some solids under irradiation. This phenomenon is termed *growth. Swelling* is the isotropic volume expansion of a solid without an external stress. *Creep* is the volume conservative distortion of a solid under an applied stress. *Growth* is the volume conservative distortion of a solid without an applied stress. Growth is only observed in non-cubic systems as it is highly dependent on anisotropy of the crystal structure. For this reason, irradiation growth can be significant in hcp metals such as zirconium and magnesium. Zirconium is stable in the α phase (hcp) below 863 °C and in the β phase (bcc) between 863 °C and T_m. Alpha-Zr has an ideal *c*/*a* ratio of 1.589. Three types of planes play key roles in the deformation and growth behavior of α-zirconium and its alloys:

- Prism I $(10\bar{1}0)$ and prism II $(11\bar{2}0)$
- Pyramidal $(11\bar{2}1), (11\bar{2}2), (10\bar{1}2)$
- Basal (0001)

Also of importance are the $(10\bar{1}2)$ and $(11\bar{2}2)$ planes. The prism, pyramidal, and basal planes are shown in Fig. 13.23.

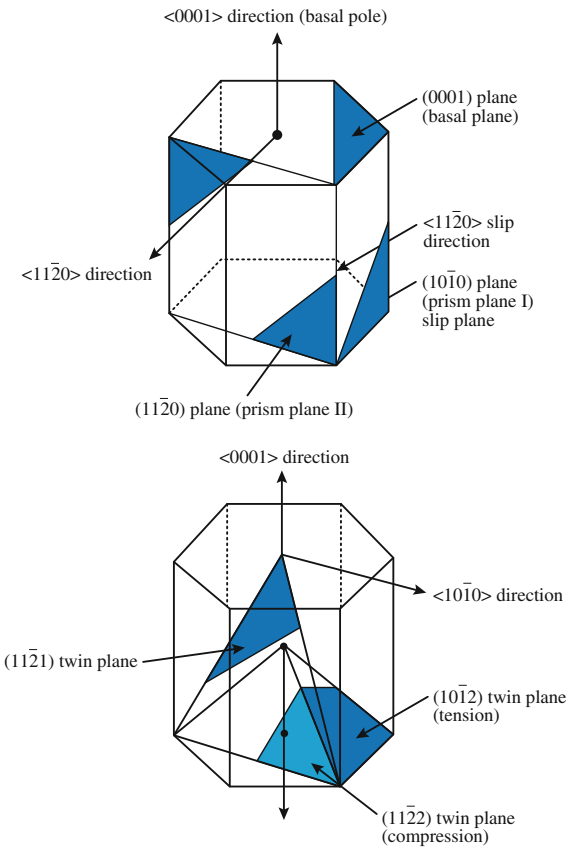

Fig. 13.23 Prism, pyramidal, and basal planes in an hcp structure (after [26])

Deformation in hcp metals occurs by both slip and twinning. For stresses along the *a*-axis, slip occurs primarily on the $(10\bar{1}0)$ prism I plane in the $\langle 11\bar{2}0\rangle$ direction. At higher stress, slip occurs on the $(10\bar{1}1)$ and $(11\bar{2}1)$ pyramidal planes and in a $\langle c + a\rangle$ direction, or along $\langle 11\bar{2}3\rangle$ At high temperatures, slip can occur on the (0001) basal plane in the *a*-direction, $\langle 1\bar{2}10\rangle$. Twinning is also a common deformation mode in hcp metals. Twinning will occur for stresses that have a component in the *c*-direction on one of the four pyramidal planes. The slip systems for deformation along the *c*-direction and as a function of temperature are given in Table 13.1. Note that different levels of stress are required to activate different deformation mechanisms. Hence, the stress needed to cause plastic deformation is a

Table 13.1 Slip systems for deformation in zirconium

	Tension (*c*-axis)		Compression (*c*-axis)	
Temp	Plane	Direction	Plane	Direction
Low	$(11\bar{2}1)$	$\langle\bar{1}\bar{1}21\rangle$	$(11\bar{2}1)$	$\langle\bar{1}\bar{1}23\rangle$
High	$(10\bar{1}2)$	$\langle\bar{1}011\rangle$	$(10\bar{1}1)$	$\langle\bar{1}012\rangle$

function of direction. A crystal possessing properties that are directionally dependent are called anisotropic.

Commercial production techniques result in Zr components in which the grains are aligned along preferential directions of the crystal. The preferential orientation of crystal directions is known as texture. The implication of texture in Zr components is that the anisotropic nature of the single crystal is exhibited in the polycrystalline material. Further, the texture changes with deformation, and this is known as texture rotation. The texture is quantified by the f_i number or the fraction of basal poles in the ith direction, where $i = L, T,$ or N for longitudinal, transverse, and normal, respectively. Note that $f_L + f_T + f_N = 1$ always.

13.3.1 Microstructure of Irradiated Zirconium Alloys

To understand growth and creep in an anisotropic solid, we must have an understanding of the nature of the irradiated microstructure. One of the prime consequences of the crystal structure of zirconium and its alloys is anisotropic diffusion [27]. Another is that the dilatational strain of the self-interstitial is smaller in Zr than in most cubic solids, resulting in smaller elastic interaction between dislocations and interstitials, which gives rise to vacancy loop stability. In fact, this small dilatational misfit may also explain the ease of Zr in accommodating interstitial gas atoms. The irradiation microstructure of Zr alloys can be summarized as follows.

Vacancy and interstitial $\langle a \rangle$-type 1/3 $\langle 1120 \rangle$ (prism plane) loops nucleate and grow during neutron irradiation. Both are present in approximately equal numbers between temperatures of 300 and 450 °C, but vacancy loops are unstable above this range due to thermal emission. The relative numbers of vacancy and interstitial loops are dependent on the proximity of biased sinks for either interstitials or vacancies. The $\langle a \rangle$-type dislocation loops arrange themselves in layers parallel to the basal plane, as shown in Fig. 13.24.

At doses above about 2.5×10^{25} n/m^2, in the temperature range 300–500 °C, $\langle c \rangle$-component dislocations start to develop on both the pyramidal and basal planes. The latter consist of vacancy loops having Burgers vector $1/6\langle 20\bar{2}3 \rangle$. The basal vacancy loops are believed to nucleate in collision cascades and owe their stability to solutes that lower the stacking fault energy and stabilize them at small size. Impurity segregation at dislocations near the loops or anisotropic diffusion is likely to be the most important factors governing loop growth. Additional factors that are important in $\langle c \rangle$-component loops are stress and the magnitude of the Burgers vector.

At all temperatures, dislocation loop growth contributes to the network during irradiation, and recovery of the dislocation network is not significant below 400 °C. The $\langle c \rangle$-component vacancy sinks are likely net vacancy sinks and $\langle c \rangle$-type dislocations are probably net interstitial sinks. The fact that $\langle c \rangle$-component loops on

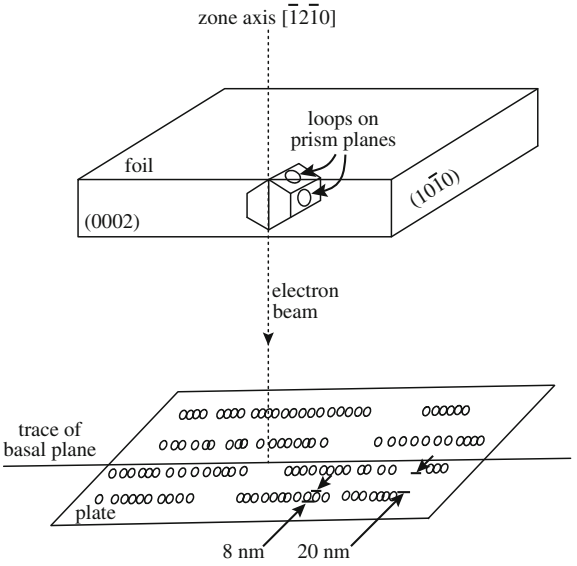

Fig. 13.24 Schematic diagram of the arrangement of dislocation loops on prism planes in irradiated zirconium (after [28])

basal planes are generally of vacancy character also indicates that the $\langle c \rangle$-component network dislocations are also vacancy sinks since they climb in a similar manner.

Grain boundaries serve as sinks for interstitial defects during irradiation of annealed Zr. The bias is dependent on the grain boundary orientation and is a minimum for boundary planes that are parallel to the basal plane (0001). Voids can form in Zr at temperatures between 350 and 500 °C, and their formation is a strong function of impurities and the presence of insoluble gases. When they form, they also tend to be located at second phase particles. In fact, the lack of insoluble gases is likely one of the reasons for the instability of voids and the stability of $\langle c \rangle$-component loops instead. As in cubic metals, insoluble gases play an important role in stabilizing small vacancy clusters against collapse to vacancy loops.

Lastly, radiation induces the formation (of ZrSn or ZrNb) or the dissolution or redistribution and reprecipitation of intermetallic phases containing Zr and Fe, Cr or Ni depending on temperature, solute content, and dose. The rebalancing of solute in the matrix can have an impact on the processes of creep and growth.

13.3.2 Irradiation Growth

Growth is easiest to understand first in single crystal zirconium. Measurements of growth of single crystal zirconium were first reported by Buckley in 1962 [29]. The shape change that occurred involved an expansion along the *a*-axis and a contraction along the *c*-axis, with magnitudes that resulted in zero net volume change,

consistent with the concept of growth as a volume conservative distortion process. Results of these observations led to one of the first models of irradiation growth which held that interstitials condensed as dislocation loops lying on the prism planes and vacancies from depleted zones collapsed to form vacancy loops lying on the basal planes. This process is equivalent to a transfer of atoms from basal planes to prism planes via the irradiation-induced point defects, as shown schematically in Fig. 13.25. The growth strains of single crystal zirconium as a function of neutron fluence are shown in Fig. 13.26 in which there is a large positive growth strain in the $\langle a \rangle$-direction, a negative growth strain in the $\langle c \rangle$-direction, and near zero strain in the $\langle c + a \rangle$-direction. But subsequent, detailed TEM observations [27, 28] of the dislocation loop structure of Zr that had undergone irradiation growth showed that all of the irradiation-induced dislocation loops had Burgers vectors of the type, $b = 1/3\langle 11\bar{2}0 \rangle$, or $\langle a \rangle$-type loops and no indication of $\langle c \rangle$-component loops. While the loops with $\langle a \rangle$-type Burgers vector could account for the a-axis expansion, they

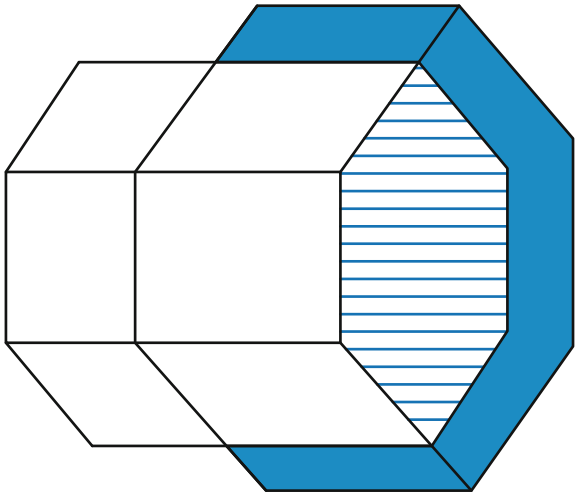

Fig. 13.25 Schematic of the change in shape of single crystal of α-zirconium produced by interstitial condensation on prism planes and vacancy-depleted zone collapse on basal planes

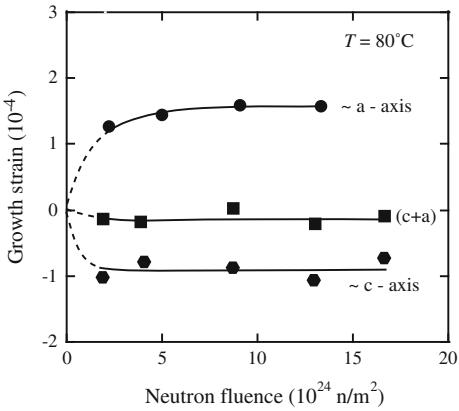

Fig. 13.26 Growth strains of annealed single crystals of zirconium as a function of neutron fluence at 80 °C (after [30])

do not account for the *c*-axis contraction. In fact, after an initial strain of about 10^{-4}, the growth quickly saturated. Irradiation to much higher doses showed that the saturation was in fact temporary and that the growth strain exhibited a *breakaway* behavior above $\sim 2.5 \times 10^{25}$ n/m^2 (Fig. 13.27). Breakaway growth has been ascribed to the nucleation and growth of $\langle c \rangle$-component vacancy loops [29]. The current evidence supports the nucleation of a low density of loops with $1/6\langle 20\bar{2}3 \rangle$ Burgers vectors that grow to relatively large sizes (>100 nm). In fact, much of the growth strain in Zircaloy-2 at high fluence can be accounted for by excess interstitial annihilation at $\langle a \rangle$-type loops and network dislocations with the corresponding vacancies annihilating at the $\langle c \rangle$-component loops [33].

In polycrystalline zirconium alloys, irradiation growth consists of three components: (1) a short-term transient due to irradiation-induced microstructure changes such as defect clusters or loops, (2) a crystallographic texture-dependent steady-state growth component, and (3) a texture-dependent long-term transient arising from breakaway growth [32]. The growth strain in a given direction of a polycrystal, ***d,*** can be related to its crystallographic texture by the *f* numbers and is proportional to the growth anisotropy factor, G_d:

$$G_d = 1 - 3f_d^b \,, \tag{13.130}$$

where f_d^b is the resolved fraction of basal poles in the direction *d*. The values of f_d^b are determined from basal pole figures obtained by X-ray diffraction using the relationship:

$$f_d^b = \sum_q V_q \cos^2 q \,, \tag{13.131}$$

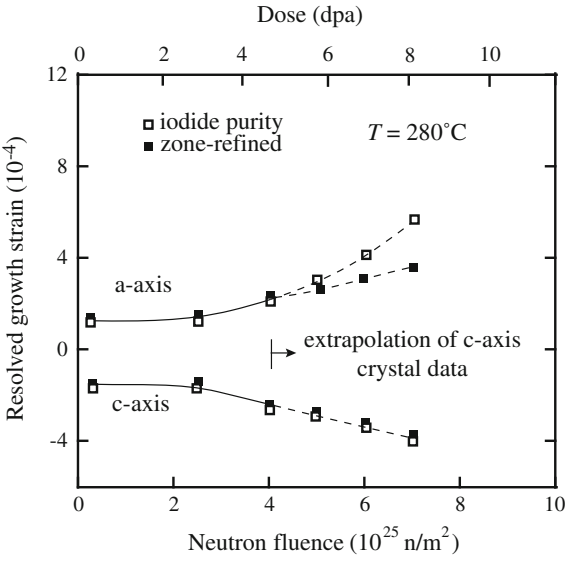

Fig. 13.27 Growth at high fluence for annealed zirconium single crystals at 273 °C showing the onset of breakaway growth at a fluence of 2.5×10^{25} n/m^2 (after [30])

where V_q is the volume fraction of grains with their basal poles at an angle q from the direction d. If the resolved fraction of basal poles in a given direction is equal to 1/3, then according to Eq. (13.130), the growth in that direction should be zero. The growth strain in the longitudinal, transverse, and thickness directions of recrystallized and cold-worked Zircaloy-2 irradiated at 287 °C and 327 °C fit the behavior rather well [35]. Figure 13.28 shows that the growth behavior of recrystallized Zircaloy-2 at 57 °C also follows Eq. (13.130).

Irradiation growth is weakly dependent on grain size with smaller grains giving rise to larger growth. It is also dependent on cold-work with higher cold-work resulting in a greater growth strain (Fig. 13.29). Growth appears to be dependent on fluence, but there is not much evidence to support a flux dependence. Finally, growth is observed to increase with temperature, with a rapid increase above about 400 °C due in part to an increase in volume. It has also been proposed that impurity elements, such as Fe, can stabilize $\langle c \rangle$-component loop embryos and enable their growth. Irradiation has been observed to amorphize Fe- and Cr-rich precipitates

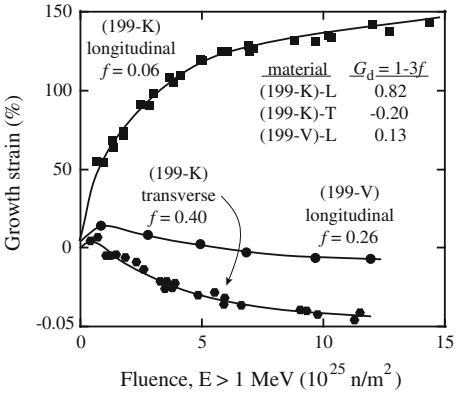

Fig. 13.28 Texture dependence of irradiation growth of Zircaloy-2 sheet at 57 °C (after [36])

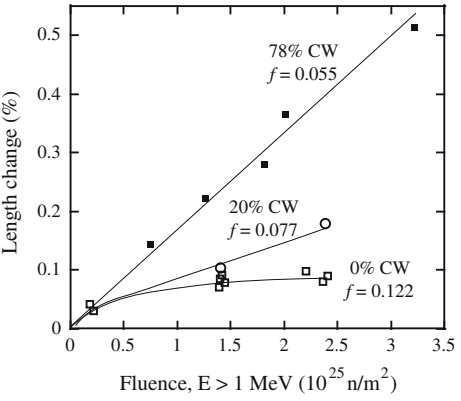

Fig. 13.29 Effect of cold-work on irradiation growth in Zircaloy-4 irradiated near 282 °C (after [34])

[37] causing the redistribution of iron into the matrix [38]. This dissolution process may be a source of iron for $\langle c \rangle$-component loop stabilization at high fluences.

A model [39] has been developed that attempts to capture the sensitivity of the growth rate to the microstructure by estimating the annihilation probabilities for interstitials and for vacancies at the various microstructural sinks. It holds that growth is driven by the difference in the anisotropy of interstitial and vacancy migration in which (1–3*f*) growth can occur in cold-worked microstructures by vacancy partitioning to the $\langle c + a \rangle$-network dislocations and interstitial partitioning to the *a*-type dislocations. The linear dependence of the growth rate of cold-worked and stress-relieved Zircaloy-2 is controlled by fast vacancy migration with a low migration energy of 0.7 eV. The breakaway growth at high fluences is due to the appearance of basal plane loops which act as strong vacancy sinks.

13.3.3 Irradiation Creep

Time-dependent deformation in zirconium alloys is a combination of thermal creep, irradiation creep, and growth. While the thermal creep component at reactor temperatures is generally small if not negligible, irradiation creep and growth components are not easily separable. The dependence of unirradiated zirconium tensile and creep properties on temperature can be subdivided into three regions as shown in Fig. 13.30. Below about 175 °C, the yield stress decreases with temperature, but creep below the yield stress does not depend strongly on temperature. Region II is the *athermal* region of creep and extends between about 175 and 523 °C in which mechanical recovery balances strain aging and the net effect is that creep is independent of temperature but does not readily reach steady-state creep. Above 523 °C, the strong dependence of yield strength on temperature and the increased recovery leads to steady-state creep rates at constant stress.

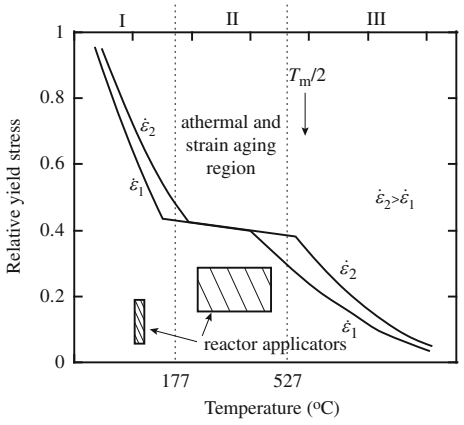

Fig. 13.30 Temperature dependence of the yield strength of zirconium alloys (after [34])

In reactor, creep follows the phenomenological equation:

$$\dot{\varepsilon} = A\sigma^n \phi^m G_d \exp(-Q/kT)[f(t) \text{ or } g(\varepsilon)] , \tag{13.132}$$

where $f(t)$ and $g(\varepsilon)$ are functions of time and strain, respectively, and other terms are as previously defined. While the flux dependence is generally taken to be linear, correlations show that the value of m varies between 0.25 and 0.85 at low fluxes (10^{16} n/m^{2}s) and rises to an asymptotic value of 1.0 at high fluxes (10^{18} n/m^{2}s) [34]. The flux exponent also was found to decrease with temperature and become negligible above 523 °C (region III) [40]. The fluence dependence is generally linear, but data exist to show that at high fluence ($> \sim 2 \times 10^{25}$ n/m^2), there is an upturn in the creep rate (Fig. 13.31).

Creep of zirconium alloys is highly dependent on the stress. At 300 °C and low stress ($<1/3\sigma_y$), $n = 1$. With increasing stress to values between 200 and 400 MPa, n rises to a value of 2 and then increases rapidly at higher stresses and can reach a value of 100 at a stress of 600 MPa (Fig. 13.32). Below about 300 °C, the temperature dependence of creep is weak and the activation energy is between 16 and 40 kJ/mol (Fig. 13.33). The temperature dependence increases rapidly with temperature, and Q can exceed 200 kJ/mol. However, the transition temperature for Q is dependent on alloy content, metallurgical condition, and stress [34]. As with growth, creep is highly dependent on the texture, which is included as the anisotropy coefficient in Eq. (13.132). However, as shown in Fig. 13.34, the texture dependence is greatest in the primary creep range. Creep in zirconium alloys is believed to be due to slip of $\langle a \rangle$-type dislocations on prism planes with secondary slip of $\langle c + a \rangle$-type dislocations on pyramidal planes. In Zircaloy-2 and Zr–2.5 % Nb, slip of $\langle a \rangle$-type dislocations contributed over 90 % of the total strain [41]. The most likely mechanism to explain creep at low stress is the SIPA mechanism. As discussed earlier, this mechanism has an $n = 1$ stress dependence, which is consistent with creep at low stress. The elastodiffusion origin of SIPA [42] in which

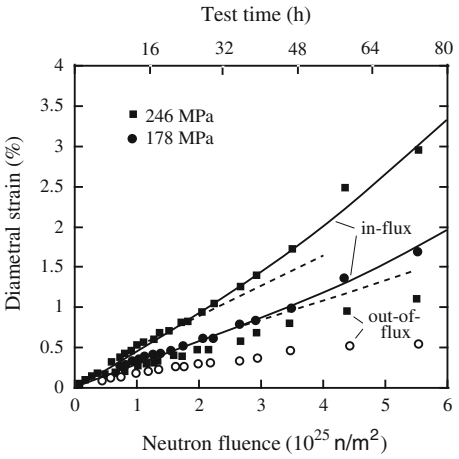

Fig. 13.31 Diametral creep strain in cold-worked Zr–1.5Nb tubes irradiated at 297 °C and a fast neutron flux of 2.1×10^{17} n/m^{2}s (after [34])

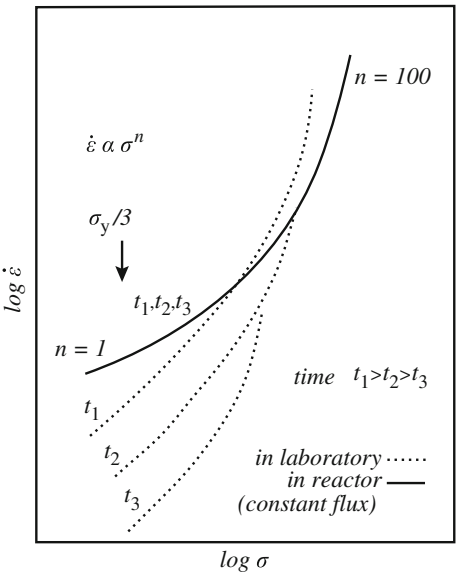

Fig. 13.32 Schematic of the stress dependence of in-reactor creep in zirconium alloys at about 300 °C (after [34])

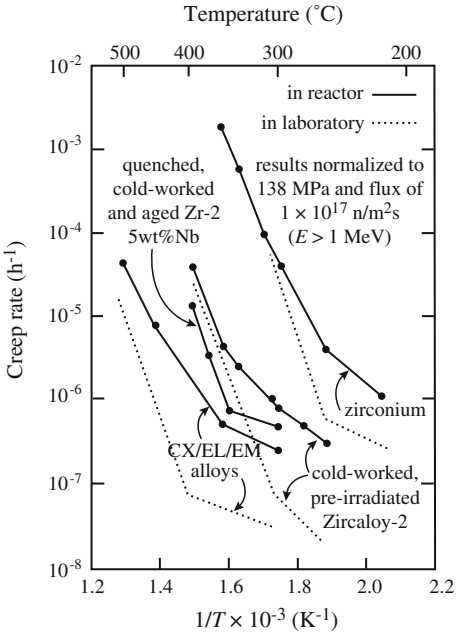

Fig. 13.33 Temperature dependence of in-reactor creep in zirconium alloys (after [34])

diffusion of interstitials is anisotropic in an applied stress field is consistent with the partitioning of interstitials to $\langle a \rangle$-type loops, facilitating their climb and glide.

A deformation-mechanism map for unirradiated Zircaloy-4 calculated assuming a grain size of 150 μm [43] is shown in Fig. 13.35. The map was drawn as contours

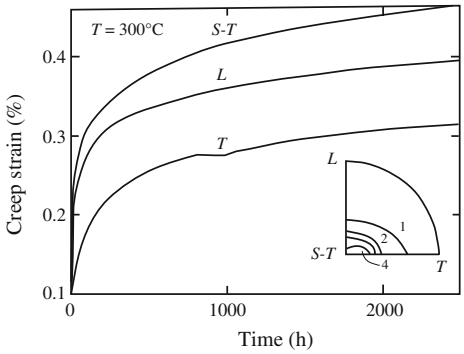

Fig. 13.34 Creep of cold-worked Zircaloy-2 at 207 MPa and 300 °C after [34]

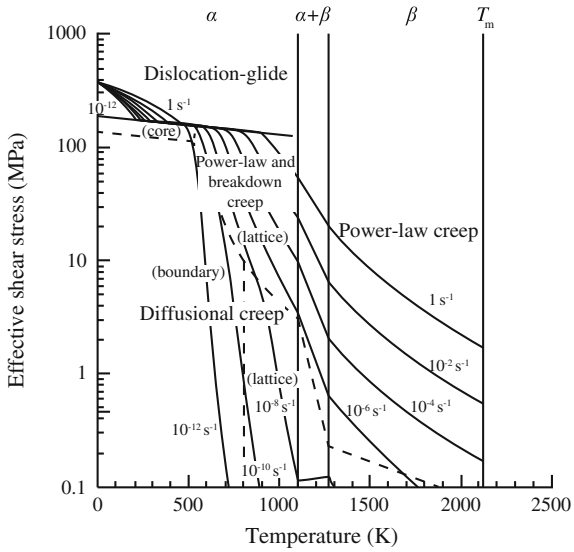

Fig. 13.35 Deformation-mechanism map for unirradiated Zircaloy-4 with a grain size of 150 μm (after [43])

of constant strain rate in a stress–temperature space. All mechanisms were assumed to act simultaneously, and the boundaries between the different mechanisms were set to where the dominant mechanisms switched. An exception to this rule was the transition to dislocation glide. For consistency between the strain rates in the different regimes, a transition stress of $\tilde{\tau}/G = 4.8 \times 10^{-3}$ was set below which dislocation glide was not active. This is equivalent to a narrow region in which the flow rate of the alloy is independent of temperature.

Nomenclature

A	Area of slip plane or dislocation loop
$\bar{A}$	Average loop area
a	Lattice constant
$\boldsymbol{b}$	Burgers vector
B_0	Creep compliance
$C_{\mathrm{v,i}}$	Concentration of vacancies, interstitials
$C^0_{\mathrm{v,i}}$	Thermal equilibrium concentration of vacancies, interstitials
d	Grain size
D	Creep-swelling coupling coefficient
D_{eff}	Effective diffusion coefficient
D_{gb}	Grain boundary diffusion coefficient
$D_{\mathrm{i,v}}$	Interstitial, vacancy diffusion coefficient
D_{vol}	Volume diffusion coefficient
e	Engineering strain
E	Energy or elastic modulus
E_{vol}	Activation energy for volume diffusion
$f^{\mathrm{b}}_{\mathrm{d}}$	Resolved fraction of basal poles in the d direction
f_{i}	Fraction of interstitial loops aligned in direction i. Also resolved fraction of basal poles of hcp unit cells in the i direction
F_{i}	Component of force in the ith direction
F_j	Frequency with which a dislocation climbs a height, h
G_{d}	Anisotropy factor
h	Obstacle height on glide plane
k	Boltzmann's constant
$k^2_{\mathrm{v,i}}$	Total sink strength for vacancies, interstitials
$k^2_{\mathrm{L,N}}$	Sink strengths for loops, networks
l	Glide length on the slip plane
J	Flux
n	The number of interstitials is required to form an interstitial loop also, number of dislocations in a pileup
n_0	Number of possible loop orientations
N	Atom number density
N_{L}	Number density of dislocation loops
P_j	Probability of a dislocation climb of j or greater
r_{c}	Dislocation core radius
r_{L}	Dislocation loop radius
R_{c}	Critical loop size for survival
R_j	Probability of finding a dislocation a distance j from unpinning point
R_{max}	Maximum dislocation loop radius
S	Loop number density
$\dot{S}$	Swelling rate
t	Time
T	Temperature
T_{m}	Melting temperature

υ_c	Dislocation climb velocity
υ_d	Average dislocation velocity
V	Volume
V_{cas}	Volume of cascade
V_q	Volume fraction of grains with their basal poles at an angle q with respect to a direction, d
$\frac{\Delta \dot{V}}{V}$	Swelling rate
$z_{i,v}^{dj}$	Capture efficiencies of dislocation of orientation j
$\Delta z_{i,v}^{d}$	Difference in capture efficiencies between aligned and non-aligned loops
α	Number of spikes per neutron scattering event, constant in Eq. (13.74)
β	Constant in Eq. (13.74)
ϕ	Neutron flux
δ	Effective thickness of the grain boundary
ε_s	Shear strain
$\dot{\varepsilon}$	Strain rate
$\dot{\bar{\varepsilon}}$	Effective strain (or creep) rate
$\dot{\varepsilon}_m$	Swelling strain
ε, ε_{ij}	Strain and components of strain
ε_e	Elastic strain
ε_{vol}	Volume strain
μ	Shear modulus
ν	Poisson's ratio
ω	Release frequency of pinned dislocation segments
Ω	Atomic volume
ρ	Total dislocation density
$\rho_{m,L,N}$	Mobile, loop, and network components of dislocation density
ρ_{FR}	Frank–Read source density
σ, σ_{ij}	Stress and components of stress
σ_s	Neutron scattering cross section. Also shear stress
$\bar{\sigma}$	Effective stress
θ	Angle between loop normal and tensile axis in (Eq. 13.74)

Subscripts

AL	Aligned loops
c	Climb
d	Dislocation
eff	Effective
FR	Frank–Read
g	Glide
gb	Grain boundary
i, v	Interstitial, vacancy
NL	Non-aligned loop
L	Loop

m	Mobile
N	Network
s	Shear
S	Swelling
vol	Volume

Superscripts

c	Compressive
dA	Aligned dislocation loops
dN	Non-aligned dislocation loops
D	Dislocation
L	Loops
V	Void
n	Stress exponent
m	Flux exponent
t	Tensile

Acronyms

GC	Glide and climb
FR	Frank–Read
N-H	Nabarro–Herring
PA	Preferential absorption
PAG	Preferential absorption glide
PE	Preferential emission
SIPA	Stress-induced preferential absorption
SIPN	Stress-induced preferential nucleation

Problems

13.1 Referring back to the void growth rate calculation in Problem 8.4 of Chap. 8:

(a) Calculate the irradiation creep rate for stainless steel as a function of temperature and applied shear stress. Assume a void number density of 2×10^{15} cm^{-3} for the creep rate calculation.

(b) Identify the window in stress–temperature space in which the creep rate remains below 0.01 %/h.

13.2 In the Hesketh model of irradiation creep by stress-enhanced vacancy–loop collapse, depleted zones with less than $m_c \sim 200$ vacancies remain in the solid as vacancy platelets. For $m < m_c$, the volume per platelet of size m is $m\Omega$. Using the inverse square distribution function for vacancy platelet (or depleted zone) size produced by a neutron collision, compute the swelling due to uncollapsed platelets in the absence of applied stress at a fast fluence

of 10^{20} neutrons/cm^2. Assume $\Sigma_s = 0.2$ cm^{-1}, $\Omega = 0.012$ nm^3, and $\nu = 500$ Frenkel pairs per fast neutron collision.

13.3 An Inconel 718 bolt is used to hold a reactor mechanical component in place. The lifetime of the bolt is determined by the stress relaxation (due to irradiation creep). The bolt must be replaced if the load drops to 10 % of the initial load. For the small irradiation dose received by the bolt, assume the creep strain rate $(\dot{\varepsilon})$ during irradiation is proportional to the displacement-damage rate $(\dot{\phi})$ and the effective stress (σ) as given in Eq. (13.124):

$$\dot{\varepsilon} = -B\dot{\phi}\,\sigma$$

(a) Calculate the radiation damage (in dpa) when the bolt stress drops to 10 % of the initial value. Assume the elastic modulus E is a constant value of 7.6×10^{10} Pa and the creep coefficient B is a constant value of 1.6×10^{-6}MPa^{-1} dpa^{-1}.

(b) Due to changes in fuel loading patterns, the dpa rate at the bolt decreases by 50 % after 5 dpa. Recalculate the total dose to reach 10 % of the initial preload. Does this change the time to replace the bolt?

13.4 A dislocation that absorbs vacancies and interstitials at different rates will exhibit climb. The climb velocity v_c is given by $v_c = (J_i^d - J_v^d)b^2$ where J_i^d is the flux of interstitials to a unit length of dislocation line and b is the Burgers vector. If the average obstacle size is 100 nm, calculate the mean time needed for dislocations to climb over obstacles in fcc aluminum at 200 °C in a monoenergetic neutron flux of 10^{14} n/cm^2 s (E = 1 MeV). Assume that the obstacles are *not* sinks for point defects and that kinetics are diffusion-limited.

$$\begin{aligned}
T_m &= 660\ ^\circ\text{C}\\
a &= 0.405\ \text{nm}\\
Q_f^v &= 3.2\ \text{eV}\\
Q_m^v &= 0.62\ \text{eV}\\
Q_f^i &= 0.66\ \text{eV}\\
Q_m^i &= 0.12\ \text{eV}\\
S_{th}^v &= 0.7k\\
S_{th}^i &= 8k\\
S_m^v &= S_m^i = 0\\
\nu &= 10^{13}\ \text{s}^{-1}\\
\rho_d &= 10^9\ \text{cm}^{-2}\\
b &= 0.2\ \text{nm}\\
z_{id} &= 1.02\\
z_{vd} &= 1.0
\end{aligned}$$

13.5 A creep experiment is performed on unirradiated 316 stainless steel (T_m = 1750 K) samples at 300 °C and 700 °C in the laboratory at low stress. Comparison experiments are performed on a second pair of 316 SS samples at the same temperatures, but *during* irradiation in a neutron flux of 1×10^{14} n/cm^{2}s ($E > 1$ MeV). A third pair of samples is tested in the laboratory at the same temperatures but after being irradiated to a fluence of 10^{21} n/cm^2 at the test temperatures.

(a) Make two plots, one for each temperature. Draw, label, and explain the expected creep curves for each of these experiments.
(b) What mechanisms would you expect to control creep in each of these experiments?

13.6 The 316 stainless steel sample irradiated at 700 °C in Problem 13.5 fails at 1 % strain in a creep test. The failure is attributed to helium embrittlement, and calculations show that the total helium content in the metal was 10^{17} at/cm^3, the grain size was 20 μm, and the swelling at failure was 30 %. What is the stress at failure?

13.7 The generalized equation for thermal creep is as follows:

$$\dot{\varepsilon} = \frac{ADμb}{kT}\left(\frac{\sigma}{\mu}\right)^n\left(\frac{b}{d}\right)^p, \quad \text{where} \quad D = D_0 \exp(-Q/kT)$$

D Diffusion coefficient
d Grain size
b Burgers vector
k Boltzmann's constant
T Temperature (K)
μ Shear modulus
σ Applied stress
n Stress exponent
p Inverse grain size exponent
A Dimensionless parameter

(a) Are any of the variables that describe the creep affected by irradiation?
(b) If so, how would increasing the displacement rate during an irradiation by an order of magnitude change the creep rate in a pure alloy with very low sink density?

13.8 The generalized correlation between creep and swelling given in Eq. (13.125) is as follows:

$$\dot{\bar{\varepsilon}}/\bar{\sigma} = B_0 + D\dot{S}$$

Comparing this equation to the generalized creep equation in Problem 13.7 implies that the stress exponent is 1. What does that tell you about the likely mechanisms of creep?

References

1. Frost HJ, Ashby MJ (1982) Deformation mechanism maps: the plasticity and creep of metals and ceramics. Pergamon, New York
2. Olander DR (1976) Fundamental aspects of nuclear reactor fuel elements, TLD-26711-Pl. Technical Information Center, ERDA, Washington Chap. 19
3. Weertman J (1955) J Appl Phys 26(10):1213
4. Weertman J (1968) Trans ASM 61:681
5. Weertman J (1957) J Appl Phys 28(3):362
6. Cadek J (1988) Creep in metallic materials. Elsevier, New York
7. Nabarro FRN (1948) Report on Conference on Strength of Solids. Physical Society, London, p 75
8. Herring C (1950) J Appl Phys 21:437
9. Coble RL (1963) J Appl Phys 34:1679
10. Brailsford AD, Bullough R (1973) Phil Mag 27:49
11. Bullough R (1985) Dislocations and properties of real materials. In: Proceedings of royal society, London, The Institute of Metals, London, p 283
12. Cheng X, Was GS (2014). J Nucl Mater 454:255–264
13. Kroupa (1966) In: Gruber B (ed) Theory of crystal defects. Adacemic Press, New York, pp 308–311
14. Matthews JR, Finnis MW (1988) J Nucl Mater 159:257–285
15. Mansur LK (1979) Phil Mag A 39(4):497
16. Wolfer WG, Foster JP, Garner FA (1972) Nucl Technol 16:55
17. Mansur LK (1992) Mater Sci Forum 97–99:489–498
18. Grossbeck ML, Mansur LK (1991) JNM 179–181:130–134
19. Brinkman JA, Wiedersich H (1964) In: Proceedings of the symposium on flow and fracture of metals and alloys in nuclear environment, STP 380. American Society for Testing and Materials, West Conshohocken, p 3
20. Mansur LK, Coghlan WA, Reiley TC, Wolfer WG (1981) J Nucl Mater 103/104:1257
21. Lewthwaite GW (1973) Scr Metal 7:75
22. Garner FA (1994) In: Frost BRT (ed) Materials science and technology, Chap. 6, vol 10A. VCH, New York, p 419
23. Cheng X, Was GS (2015) J Nucl Mater 459:183
24. Garner FA, Grossbeck ML (1994) Fusion materials semi-annual progress report DE/ER-0313/16. US DOE, Oak Ridge, TN, Mar 1994
25. Zinkle S, Lucas GE (2003) Deformation and fracture mechanisms in irradiated FCC and BCC metals, US department of energy, semi-annual report, DOE-ER-0313/34. US DOE, Washington, DC
26. Klepfer HH (ed) (1962) Proceedings of the USAEC symposium on zirconium alloy development, US Atomic Energy Commission, GEAP4089, vol II, p 13–11
27. Griffiths M (1988) J Nucl Mater 159:190
28. Northwood DO (1977) At Energy Rev 15(4):547
29. Buckley SN (1962) Uranium and graphite. Institute of Metals, London, p 445
30. Carpenter GJC, Zee RH, Rogerson A (1988) J Nucl Mater 159:86
31. Fidleris V (1975) At Energy Rev 13:51
32. Northwood DO, Fidleris V, Gilbert RW, Carpenter GJC (1976) J Nucl Mater 61:123
33. Griffiths M, Gilbert RW (1987) J Nucl Mater 150:169
34. Fidleris V (1988) J Nucl Mater 159:22
35. Adamson RB, Tucker RP, Fidleris V (1982) Zirconium in the nuclear industry the 5th symposium, STP 754. American Society for Testing and Materials, West Conshohocken, p 208
36. Fidleris V, Tucker RP, Adamson RB (1987) Zirconium in the nuclear industry the 7th symposium, STP 939. American Society for Testing and Materials, West Conshohocken, p 49
37. Lemaignan C, Motta AT (1994) In: Frost BRT (ed) Materials science and technology, vol 10B. VCH, New York, p 1 Chap. 7

38. Zu XT, Sun K, Atzmon M, Wang LM, You LP, Wan FR, Busby JT, Was GS, Adamson RB (2005) Phil Mag 85(4–7):649–659
39. Holt RA (1988) J Nucl Mater 159:310
40. Nichols FA (1969) J Nucl Mater 20:249
41. Christodoulou N, Causey AR, Woo CH, Tome CN, Klassen RJ, Holt RA (1993) In: Kumar AS, Gelles DS, Nanstad RK, Little EA (eds) Proceedings of the 16th international symposium on effects of radiation on materials, ASTM STP 1175. American Society for Testing and Materials, West Conshohocken, pp 1111–1128
42. Woo CH (1984) J Nucl Mater 120:55
43. Wang H, Hu Z, Lu W, Thouless MD (2013) J Nucl Mater 433:188